We are IntechOpen, the world's leading publisher of Open Access books
Built by scientists, for scientists

4,800
Open access books available

122,000
International authors and editors

135M
Downloads

Our authors are among the

154
Countries delivered to

TOP 1%
most cited scientists

12.2%
Contributors from top 500 universities

CLARIVATE ANALYTICS
BOOK CITATION INDEX
INDEXED

WEB OF SCIENCE™

Selection of our books indexed in the Book Citation Index
in Web of Science™ Core Collection (BKCI)

Interested in publishing with us?
Contact book.department@intechopen.com

Chapter

Very Compact Linear Colliders Comprising Seamless Multistage Laser-Plasma Accelerators

Kazuhisa Nakajima, Min Chen and Zhengming Sheng

Abstract

A multistage laser-plasma accelerator (LPA) driven by two mixing electromagnetic hybrid modes of a gas-filled capillary waveguide is presented. Plasma wakefields generated by a laser pulse comprising two mixing modes coupled to a metallic or dielectric capillary filled with gas provide us with an efficient accelerating structure of electrons in a substantially long distance beyond a dephasing length under the matching between a capillary radius and plasma density. For a seamless multistage structure of the capillary waveguide, the numerical model of the transverse and longitudinal beam dynamics of an electron bunch considering the radiation reaction and multiple Coulomb scattering effects reveals a converging behavior of the bunch radius and normalized emittance down to ~1 nm level when the beam is accelerated up to 560 GeV in a 67 m length. This capability allows us to conceive a compact electron-positron linear collider providing with high luminosity of 10^{34} cm^{-2} s^{-1} at 1 TeV center-of-mass (CM) energy.

Keywords: future colliders, lepton colliders, laser-plasma accelerators, multistage coupling, CAN lasers

1. Introduction

In the long-standing quest for the fundamental building blocks of nature, the so-called Standard Model of particle physics, energy frontier colliders have played a central role in the forefront research for matter and interactions. For future high-energy particle colliders to explore physics beyond the Standard Model, a proton-proton circular collider at energy of 100 TeV in a 100 km circumference or electron-positron linear collider with energy of the order of 1 TeV in a 30 km length is being considered around the world, exploiting the conventional technologies such as superconducting magnets or RF systems [1]. In contrast to proton colliders that create clouds of debris, electron-positron colliders enable cleaner and more precision experiments of fundamental particle collisions. Nowadays, a diversity of electron-positron linear colliders is proposed as a potential application of advanced accelerator concepts [2], such as two beam accelerators, dielectric wakefield accelerators, beam-driven plasma wakefield accelerators, and laser-driven plasma wakefield accelerators [3], promising with much higher accelerating gradients than that of a conventional RF accelerator.

Laser-plasma accelerators (LPAs) [4, 5] can support a wide range of potential applications requiring high-energy and high-quality electron-positron

beams. In particular, field gradients, energy conversion efficiency, and repetition rates are essential factors for practical applications such as compact free electron lasers [6, 7] and high-energy frontier colliders [8, 9]. Although LPAs provide enormous accelerating gradients, as high as 100 GV/m at the plasma density of 10^{18} cm^{-3}, dephasing of relativistic electrons with respect to a correct acceleration phase of the plasma wakefield with the phase velocity that is smaller than the speed of light in vacuum, and energy depletion of the laser pulse limit the electron energy gain in a single stage. A straightforward solution to overcome the dephasing and pump depletion effects is to build a multistage accelerator comprising consecutive LPA stages [3] such that a final energy gain reaches the requirement of the beam energy without loss of the beam charge and qualities through a coupling segment where a fresh laser pulse is fed to continuously accelerate the particle beam from the previous stage. The propagation of laser pulses in plasmas is described by refractive guiding, in which the refractive index can be modified from the linear free space value mainly by relativistic self-focusing, ponderomotive channeling, and a preformed plasma channel [10]. The self-guided LPA [11–14] relies only on intrinsic effects of relativistic laser-plasma interactions such as relativistic self-focusing and ponderomotive channeling. On the other hand, the channel-guided LPA exploits a plasma waveguide with a preformed density channel [15–17] or a gas-filled capillary waveguide made of metallic or dielectric materials [18]. The plasma waveguide is likely to propagate a single-mode laser pulse through a radially parabolic distribution of the refractive index and generates plasma waves inside the density channel, the properties of which are largely affected by a plasma density profile and laser power [19]. In contrast with plasma waveguides, the capillary waveguide can guide the laser due to Fresnel reflection on the inner capillary wall, and plasma waves are generated in an initially homogeneous plasma, relying on neither laser power nor plasma density. The presence of the modal structure imposed by the boundary conditions at the capillary wall affects the propagation of a laser pulse through the capillary and thus the excitation of plasma waves inside the capillary. This characteristic allows us to control acceleration of electrons through the modal structure of the propagation of the laser pulse as long as the laser intensity on the capillary wall is kept below the material breakdown [20, 21].

In this paper, we present a novel scheme of a gas-filled capillary accelerator driven by a laser pulse formed from two-mode mixing of the capillary eigenmodes, so-called electromagnetic hybrid modes [20]. Two coupled eigenmodes with a close longitudinal wave number can generate beating wakefields in the capillary. When the beating period is equal to the dephasing distance, the electrons experience the rectified accelerating field; thereby their energy gain can increase over many accelerating phases exceeding the linear dephasing limit and reach the saturation due to the energy depletion of a drive laser pulse in the single-stage LPA. For efficient acceleration of the electron-positron beam up to an extremely high energy such as TeV energies, the multistage accelerator comprising a series of plasma-filled capillary waveguides is a sound approach, in which the particle beam is injected into the initial stage at the right phase of the wakefield from the external injector and accelerated cumulatively in the consecutive accelerating phase of successive stages. For applications of extreme high-energy particle beams to TeV center-of-mass (CM) energy electron-positron linear colliders, minimizing the transverse normalized emittance of the beam particles is of essential importance to meet the requirement of the luminosity of the order of 10^{34} cm^{-2} s^{-1} at 1 TeV CM energy for the particle physics experiments [22]. The numerical model on the bunched beam dynamics in laser wakefields, based on the exact solution of single particle betatron motion taking into account the radiation reaction and multiple Coulomb scattering, reveals that the transverse normalized emittance and beam radius can be

consecutively reduced during continuous acceleration in the presence of optimally phased recurrence of longitudinal and transverse wakefields [19]. The final properties of the particle beams reached to the objective energy meet the requirements of the luminosity without resort to an additional focusing system.

The remaining part of this paper is organized as follows. In Section 2, the complete description on the longitudinal and transverse laser wakefields generated by two electromagnetic hybrid modes with moderate intensities coupled to a gas-filled capillary waveguide is provided. In Section 3, the particle beam dynamics on energy gain, beam loading, and betatron motion in a single stage of the two-mode mixing LPA is investigated, taking into account radiation reaction and multiple Coulomb scattering with plasma ions. In Section 4, a multistage coupling with a variable curvature plasma channel is presented. For the multistage comprising two-mode mixing LPAs, the results of numerical studies on the transverse beam dynamics of a particle bunch are shown. Analytical consideration on the evolution of the normalized emittance of the particle beam in the presence of radiation reaction and the multiple Coulomb scattering is given. In Section 5, the performance of a 1-TeV CM energy electron-positron collider comprising the multistage two-mode mixing LPAs is discussed on the luminosity and beam-beam interaction. In Section 6, we conclude our investigation on the proposed laser-plasma linear collider with a summary.

2. Laser pulse propagation in a gas-filled capillary tube

For a large-scale accelerator complex such as the energy frontier particle beam colliders, it is axiomatically useful in assembling a long-range multistage structure for the use of long-term experimental operation at a high-precision and high-repetition rate that each electromagnetic waveguide consists of a simple monolithic structure, as referred to the design of the future electron-positron linear colliders based on radio-frequency technologies [22]. Despite the long-standing research on plasma waveguides comprising density channels generated in plasmas with laser-induced hydrodynamic expansion [23, 24] and pulsed discharges of an ablative capillary [25, 26] or a gas-filled capillary [27, 28], a length of such a plasma channel has been limited to about 10 cm. The pulsed discharge capillaries relying on collisional plasma processes have some difficulties in plasma densities less than 10^{17} cm^{-3} and the temporal and spatial stabilities of the density channel properties for the operation at a high repletion rate such as 10 kHz [5, 29]. In contrast to pulsed discharge plasma waveguides, metallic or dielectric capillary waveguides filled with gas [18, 30] will be revisited for a large-scale laser-plasma accelerator operated at a practically higher-repetition rate than 10 kHz, because of the passive optical guiding of laser pulses, the propagating electromagnetic fields of which are simply determined the boundary conditions on a static solid wall of the waveguide unless the laser intensity is high enough to cause the material breakdown on a capillary wall [20, 21]. Furthermore, the modal nature of electromagnetic fields arising from the boundary conditions on a solid wall allows us to conceive a novel scheme that can overcome a drawback of LPAs, referred to as dephasing of accelerated electron beams from a correct acceleration phase in laser wakefields.

2.1 Laser-driven wakefields generated by two capillary modes

Considering the electromagnetic hybrid modes EH$_{1n}$ [20] to which the most efficient coupling of a linearly polarized laser pulse in vacuum occurs, the normalized vector potential for the eigenmode of the n-th order is written by [31].

$$a_n = a_{n0}J_0(u_n r/R_c) \exp\left[-k_n^l z - \frac{(z - v_{g,n}t)^2}{2c^2\tau^2}\right]\cos(\omega_0 t - k_{zn}z), \qquad (1)$$

where a_{n0} is the amplitude of the normalized vector potential defined as $a_{n0} \equiv eA_{n0}/m_e c^2$ for the EH_{1n} mode with the vector potential A_{n0}, the electron charge e, electron mass m_e, and the speed of light in vacuum c; J_0 the zero-order Bessel function of the first kind; u_n the n-th zero of J_0; r the radial coordinate of the capillary in cylindrical symmetry; R_c the capillary radius; z the longitudinal coordinate; τ the pulse duration; and ω_0 the laser frequency. The longitudinal wave number k_{zn}, the damping coefficient k_n^l, and the group velocity of the n-th mode $v_{g,n}$ are given by [20].

$$k_{zn} = \left(k_0^2 - \frac{u_n^2}{R_c^2}\right)^{1/2}, k_n^l = \frac{u_n^2(1 + \varepsilon_r)}{2k_{zn}^2 R_c^3(\varepsilon_r - 1)^{1/2}}, v_{g,n} \simeq c\left(1 - \frac{u_n^2}{k_0^2 R_c^2}\right)^{1/2}, \qquad (2)$$

where $k_0 = \omega_0/c = 2\pi/\lambda_0$ is the laser wavenumber with the laser wavelength λ_0 and ε_r is the relative dielectric constant. In the quasi-linear wakefield regime $|\mathbf{a}| = e|\mathbf{A}|/(m_e c^2) \sim 1$, the ponderomotive force exerted on plasma electrons by two coupled capillary laser fields $\mathbf{a}_{nm} = \mathbf{a}_n + \mathbf{a}_m$ can be written by $\mathbf{F}_p = -m_e c^2 \beta_g \nabla a_{nm}^2/2$, where a_{nm}^2 is defined by averaging the nonlinear force over the laser period $2\pi/\omega_0$, i.e., assuming that $v_{g,n} \sim v_{g,m} \sim v_g$ in the propagation distance $z \leq z_{\mathrm{mix}} \approx 8\pi^2(R_c/\lambda_0)^2 c\tau/(u_m^2 - u_n^2)$, where z_{mix} is the mode mixing length over which two hybrid modes EH_{1n} and EH_{1m} overlap to cause the beatings of the normalized vector potential, e.g., $z_{\mathrm{mix}} \sim 56$ cm for the EH_{11} - EH_{12} mode mixing of a laser pulse with $\tau = 25$ fs and $\lambda_0 = 1$ μm in a capillary tube with $R_c = 152.6$ μm

$$a_{nm}^2(r,t) = \frac{1}{2}a_{n0}^2 J_0^2\left(\frac{u_n r}{R_c}\right)\exp\left[-2k_n^l z - \frac{(z - v_g t)^2}{c^2\tau^2}\right] + \frac{1}{2}a_{m0}^2 J_0^2\left(\frac{u_m r}{R_c}\right)\exp\left[-2k_m^l z - \frac{(z - v_g t)^2}{c^2\tau^2}\right]$$

$$+ a_{n0}a_{m0}J_0\left(\frac{u_n r}{R_c}\right)J_0\left(\frac{u_m r}{R_c}\right)\exp\left[-\left(k_n^l + k_m^l\right)z - \frac{(z - v_g t)^2}{c^2\tau^2}\right]\cos(k_{zm} - k_{zn})z. \qquad (3)$$

The electrostatic potential $\Phi(r,t)$ defined by $\mathbf{F}(r,t) = -e\nabla\Phi(r,t)$ is obtained from Eq. (5).

$$\left(\frac{\partial^2}{\partial t^2} + \omega_p^2\right)\Phi(r,t) = \frac{\omega_p^2 m_e c^2 \beta_g}{2e}a_{nm}^2(r,t) \qquad (4)$$

where $\omega_p = (4\pi e^2 n_e/m_e)^{1/2}$ is the plasma frequency. The solution of Eq. (4) is

$$\Phi(r,t) = \frac{\sqrt{\pi}}{8}\left(\frac{m_e c^2}{e}\right)\beta_g k_p c\tau e^{-\left(\frac{k_p c\tau}{2}\right)^2}\left[a_{n0}^2 J_0^2\left(\frac{u_n r}{R_c}\right)e^{-2k_n^l z} + a_{m0}^2 J_0^2\left(\frac{u_m r}{R_C}\right)e^{-2k_m^l z}\right.$$

$$\left. + 2a_{n0}a_{m0}J_0\left(\frac{u_n r}{R_c}\right)J_0\left(\frac{u_m r}{R_c}\right)e^{-(k_n^l + k_m^l)z}\cos\Delta k_{znm}z\right]\left[S(z)\cos k_p(z - v_g t) + C(z)\sin k_p(z - v_g t)\right], \qquad (5)$$

where $k_p = \omega_p/v_g$ is the plasma wavenumber in the capillary, $\beta_g = v_g/c$, $\Delta k_{znm} = k_{zn} - k_{zm}$ the mode beating wavenumber and

4

$$C(z) = \Re \text{erf}\left(\frac{z - v_g t}{c\tau} + i\frac{k_p c\tau}{2}\right) - 1, \quad S(z) = \Im \text{erf}\left(\frac{z - v_g t}{c\tau} + i\frac{k_p c\tau}{2}\right), \qquad (6)$$

with the real ($\Re$) and imaginary ($\Im$) part of the error function $\text{erf}(z) = (2/\sqrt{\pi})\int_0^z e^{-s^2} ds$ [5]. For k_n^l, $k_m^l \ll k_p$ and $\Delta k_{znm} \ll k_p$, the longitudinal electric field generated by the laser pulse can be obtained from $E_{zL} = -\partial\Phi/\partial z$ as

$$E_{zL}(r,z,t) = \frac{\sqrt{\pi}}{8}\left(\frac{m_e c\omega_p}{e}\right)k_p c\tau e^{-\left(\frac{k_p c\tau}{2}\right)^2}\left[a_{n0}^2 J_0\left(\frac{u_n r}{R_c}\right)e^{-2k_n^l z} + a_{m0}^2 J_0\left(\frac{u_m r}{R_c}\right)e^{-2k_m^l z}\right.$$
$$\left. + 2a_{n0}a_{m0}J_0\left(\frac{u_n r}{R_c}\right)J_0\left(\frac{u_m r}{R_c}\right)e^{-(k_n^l+k_m^l)z}\cos\Delta k_{znm}z\right]\left[S(z)\sin k_p(z-v_g t) - C(z)\cos k_p(z-v_g t)\right].$$
$$(7)$$

The transverse focusing force is obtained from $F_{rL} = e(E_r - B_\varphi) = -\partial\Phi/\partial r$ as

$$F_{rL}(r,z,t) = \frac{\sqrt{\pi}}{4}\left(\frac{m_e c\omega_p}{e}\right)\frac{c\tau}{R_c}e^{-\left(\frac{k_p c\tau}{2}\right)^2}\left[a_{n0}^2 u_n J_0\left(\frac{u_n r}{R_c}\right)J_1\left(\frac{u_n r}{R_c}\right)e^{-2k_n^l z} + a_{m0}^2 u_m J_0\left(\frac{u_m r}{R_c}\right)J_1\left(\frac{u_m r}{R_c}\right)e^{-2k_m^l z}\right.$$
$$\left. + a_{n0}a_{m0}\left(u_n J_0\left(\frac{u_m r}{R_c}\right)J_1\left(\frac{u_n r}{R_c}\right) + u_m J_0\left(\frac{u_n r}{R_c}\right)J_1\left(\frac{u_m r}{R_c}\right)\right)e^{-(k_n^l+k_m^l)z}\cos\Delta k_{znm}z\right]$$
$$\times\left[C(z)\sin k_p(z-v_g t) + S(z)\cos k_p(z-v_g t)\right],$$
$$(8)$$

where $J_1(z) = -J_0'(z)$ is the Bessel function of the first order.

The proposed scheme restricts the laser intensity such that the plasma response is within the quasi-linear regime, i.e., $a_0 \sim 1$, for two reasons. The one is avoidance of the nonlinear plasma response such as in the bubble regime, where symmetric wakefields for the electron and positron beams cannot be obtained for the application to electron-positron colliders [8, 9] and the degradation of the beam quality due to the self-injection of dark currents from the background plasma electrons. The other is an inherent demand that the laser intensity guided in a capillary tube should be lower enough than the threshold of material damage on the capillary wall [19].

### 2.2 Coupling control for generating two capillary modes

The coupling efficiency C_n defined by an input laser energy with a spot radius r_0 and amplitude a_0 coupled to the E_{1n} mode in the capillary with the radius R_c, i.e., $a_{n0}^2 = C_n a_0^2$ is calculated for a linearly polarized Airy beam,

$$C_n = \frac{4}{J_1^2(u_n)}\left[\int_0^1 J_1\left(\frac{\nu_1 R_c x}{r_0}\right)J_0(u_n x)dx\right]^2, \qquad (9)$$

and for a Gaussian beam,

$$C_n = 8\left(\frac{R_c}{r_0 J_1(u_n)}\right)^2\left[\int_0^1 x\exp\left(-\frac{x^2 R_c^2}{r_0^2}\right)J_0(u_n x)dx\right]^2, \qquad (10)$$

where $\nu_1 = 3.8317$ is the first root of the equation of $J_1(x) = 0$ [20], as shown in **Figure 1a** and **b**, respectively, as a function of R_c/r_0. In Eq. (5), the beating term can be maximized by setting R_c/r_0 at which $(C_n C_m)^{1/2}$ has the maximum value and the minimum fraction of higher-order modes. As shown in **Figure 1**, the Airy beam generates the maximum EH_{11}-EH_{12} mode mixing with $(C_1 C_2)^{1/2} = 0.45$ and a fraction of higher-order modes with ~0.5% at $R_c/r_0 = 1.67$, where the coupling
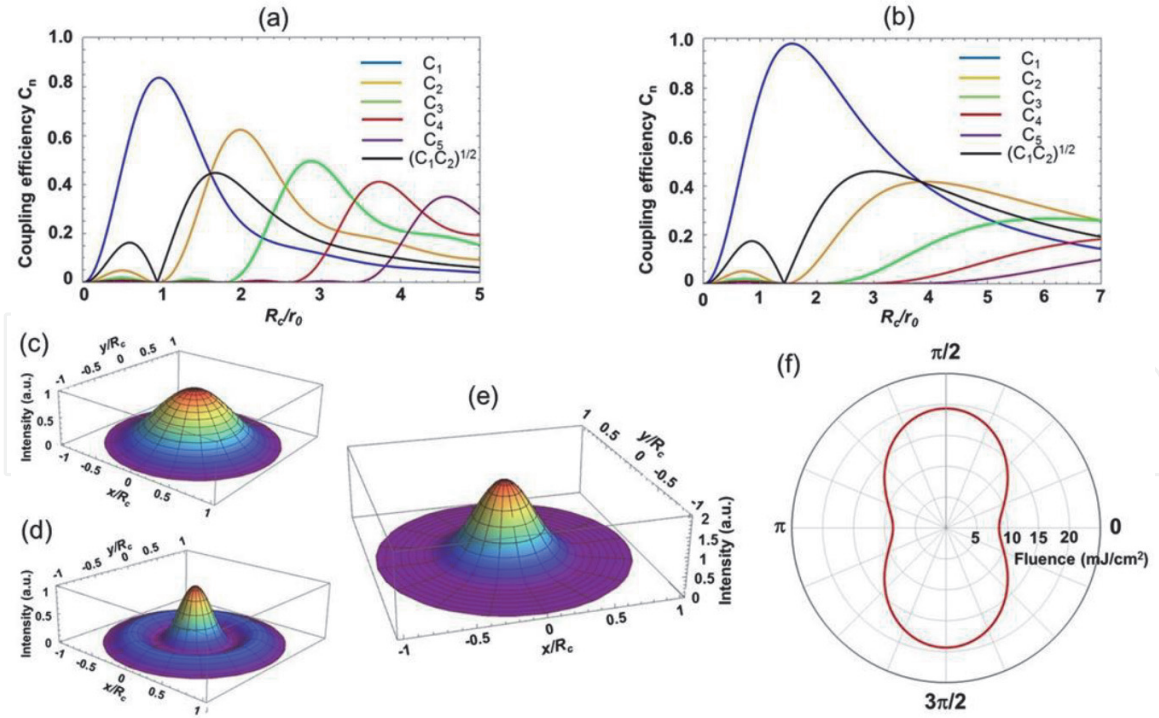
Figure 1.
(a and b) coupling efficiency C_n for an airy beam and a Gaussian beam with a spot radius r_0, respectively, coupled to the electromagnetic hybrid mode EH_{1n} in a capillary tube with a radius R_c. (c, d, and e) radial intensity profiles for the EH_{11}, EH_{12} monomode, and EH_{11}-EH_{12} mixing mode for the airy beam case. (f) Energy fluence traversing the capillary wall on $R_c = 152.6$ μm for the peak intensity $I_L = 1.37 \times 10^{18}$ W/cm² ($a_0^2 = 1$) and the pulse duration $\tau_L = 25$ fs.

efficiencies are $C_1 = 0.4022$, $C_2 = 0.4986$, $C_3 = 0.002366$, $C_4 = 0.001219$, and $C_5 = 0.000701$. The Gaussian beam can generate the EH_{11}-EH_{12} mode mixing with $(C_1 C_2)^{1/2} = 0.46$ and a fraction of higher-order modes with ~5.1% at $R_c/r_0 = 3.0$, where the coupling efficiencies are in the order of $C_1 = 0.5980$, $C_2 = 0.3531$, $C_3 = 0.04706$, $C_4 = 0.001815$, and $C_5 = 0.000022$.

The radial intensity profiles for the EH_{11}, EH_{12} monomode and EH_{11}-EH_{12} mixing mode for the Airy beam case are illustrated in **Figure 1c–e**, respectively. As shown in **Figure 1e**, a high-intensity region of the mixing mode is confined within a half radius of the capillary, compared to the monomode intensity profiles, which have a widespread robe toward the capillary wall. A centrally concentrated intensity profile of the mixing mode considerably decreases the energy flux traversing on the capillary wall. The normalized flux for EH_{1n} mode at the capillary wall depends on the azimuthal angle θ as $F_w^n = [u_n J_1(u_n)/k_0 R_c]^2 (\cos^2\theta + \varepsilon_r \sin^2\theta)/(\varepsilon_r - 1)^{1/2}$, defined by the ratio of the radial component of the Poynting vector at $r = R_c$ to the longitudinal component of the on-axis Poynting vector [20]. For the Airy beam with $\lambda_0 = 1$ μm coupled to the capillary with $\varepsilon_r = 2.25$ and $R_c = 152.6$ μm, the maximum normalized fluxes for the EH_{11}, EH_{12} mono- and EH_{11}-EH_{12} mixing modes at $\theta = \pi/2$ or $3\pi/2$ are 1.37×10^{-6}, 3.85×10^{-6}, and 6.26×10^{-7}, respectively. The energy fluence traversing the capillary wall can be estimated by $\mathcal{F}_{wall} \sim F_w^n I_L \tau_L$ for the peak intensity $I_L = 1.37 \times 10^{18}$ W/cm² ($a_0^2 = 1$) and the pulse duration $\tau_L = 25$ fs, providing the maximum fluences 19, 66, and 19 mJ/cm² for the corresponding modes, as shown in **Figure 1f**. The experimental study of laser-induced breakdown in fused silica (SiO_2) [32] suggests that the fluence breakdown threshold is scaled to be $\mathcal{F}_{th} \sim 120 - 160$ J/cm² for $\tau_L = 25$ fs. According to a more detailed study of laser propagation in dielectric capillaries under non-ideal

coupling conditions [33], the threshold intensity for wall ionization is obtained as $I_{th} \sim 2.3 \times 10^{18}\,\mathrm{W/cm^2}$ ($a_0 \simeq 1.3$) at the wavelength $\lambda_0 = 1\,\mu\mathrm{m}$ for the capillary radius $R_c = 152.6\,\mu\mathrm{m}$.

The coupling efficiency of an incident laser pulse to a capillary tube filled with plasma can be improved by the use of a cone-shape entrance of the capillary [34], suppressing self-focusing effects and increasing the accelerating wakefield excited in the capillary. For the propagation of a laser beam with an approximately Gaussian intensity profile $|a|^2 \sim a_0^2 (r_0^2/r_s^2) \exp\left(-2r^2/r_s^2\right)$, the evolution of a normalized spot radius $R = r_s/r_0$ can be obtained from the equation $d^2R/dz^2 = 1/(Z_R^2 R^3)(1 - P/P_c)$ [35], where $Z_R = k_0 r_0^2/2$ is the vacuum Rayleigh length, P the laser power, and P_c the critical power for relativistic self-focusing with $P/P_c = k_p^2 r_0^2 a_0^2/32$. For the coupling of an Airy beam (or a Gaussian beam) with the radius $r_0 = R_c/1.67$ ($R_c/3$) to the capillary tube filled with plasma at the electron density of $n_e = 1 \times 10^{18}\,\mathrm{cm^{-3}}$, the cone with the opening radius of $r_i = r_0(P/P_c)^{1/2} \sim 3r_0$ ($1.7r_0$) and length $z_c = (Z_R/2)(P/P_c - 1)^{1/2} \sim 1.43Z_R$ ($\sim 0.68Z_R$) can effectively guide and collect the incident laser energy. The effect of the relativistic self-focusing is estimated by considering the modulation of the refractive index for the $\mathrm{EH_{1n}}$ mode, i.e., $\eta_n = 1 - \omega_p^2/(2\omega_0^2)(1 - \delta\phi + \Delta_n) - u_n^2/(2k_0^2 R_c^2)$ [31], where $\delta\phi = e\Phi/m_e c^2 \simeq a^2/4 - \delta n/n_0$ [36] and $\Delta_n \sim 3C_n^2/32 - 5C_n^3/128$. The maximum modulation due to the relativistic self-focusing effect is at most 0.5% for the propagation of the $\mathrm{EH_{11}}$-$\mathrm{EH_{12}}$ mixing modes in a capillary.

3. Beam dynamics in a single-stage two-mode mixing LPA

3.1 Electron acceleration

In the linear wakefields excited by two coupled modes $\mathrm{EH_{11}}$ and $\mathrm{EH_{12}}$ in the capillary waveguide, the longitudinal motion of an electron traveling along the capillary axis at a normalized velocity $\beta_z = v_z/c \approx 1$ is described as [5].

$$d\gamma/dz = -k_p E_{z0}/E_0, \quad d\Psi/dz \approx k_p\left(1 - \beta_g\right) \approx k_p/\left(2\gamma_g^2\right), \tag{11}$$

where $m_e c^2 \gamma$ is the electron energy, $E_{z0} = E_{zL}(0, z, t)$ the accelerating field at $r = 0$, $E_0 = m_e c \omega_p/e$ the nonrelativistic wave-breaking field, $\Psi \simeq k_p\left(z - v_g \int_0^z dz/v_z\right)$ the particle phase with respect to the plasma wave, and $\gamma_g = \left(1 - \beta_g^2\right)^{-1/2} \gg 1$. Here, the phase-matching condition is determined such that the beating wavelength is equal to the dephasing length, i.e., $L_{dp} = \lambda_p \gamma_g^2/2 = \pi/(2\Delta k_{z12})$

$$\Delta k_{z12} = k_{z1} - k_{z2} \approx \left(u_2^2 - u_1^2\right)/\left(2k_0 R_c^2\right) = k_p/\left(2\gamma_g^2\right). \tag{12}$$

Taking into account $C(z) \to -2$ and $S(z) \to 0$ for $z - v_g t \ll -c\tau$ and setting the pulse duration of a drive laser pulse with a Gaussian temporal profile to be the optimum length $k_p c \tau = \sqrt{2}$, the on-axis accelerating field near the matching condition is given by

$$E_{z0}/E_0 = -\sqrt{\pi/8}a_0^2 e^{-\left(1 + 4\alpha_d a_0^2 \Psi\right)/2}\left[C_1 + C_2 + 2\sqrt{C_1 C_2}\cos\left(\Psi + \delta\right)\right]\cos\Psi, \tag{13}$$

where $\delta = \left(\Delta k_{z12} - k_p/2\gamma_g^2\right)L_{dp} \sim \pi\left[\left(u_2^2 - u_1^2\right)\gamma_g^3/\left(k_0{}^2 R_c^2\right) - 1\right]/2$ is a phase mismatching.

While propagating through plasma and generating wakefields, the laser pulse loses its energy as $\partial\mathcal{E}_L/\partial z \sim -\mathcal{E}_L/L_{\rm pd}$ [37] where $L_{\rm pd}$ is the characteristic scale length of laser energy deposition into plasma wave excitation, referred to as the pump depletion length. In the linear wakefield regime where a laser pulse duration is assumed to be fixed, the laser energy evolution in the capillary can be written as $\mathcal{E}_L(z) \propto a_0^2(C_1 + C_2)e^{-z/L_{\rm pd} - 2\left(k_1^l + k_2^l\right)z}$, taking into account the energy attenuation of two coupled hybrid modes. In the quasi-linear wakefield regime, i.e., $a_0^2 \lesssim 1$, the scaled pump depletion length is given by $k_p L_{\rm pd} = \gamma_g^2/\left(\alpha_d a_0^2\right)$ with $\alpha_d \simeq (C_1 + C_2)/17.4$ for a Gaussian laser pulse [9, 37], while the scaled coupled mode attenuation length yields $k_p/2\left(k_1^l + k_2^l\right) \sim 0.35\gamma_g^{7/2}u_2 \gg k_p L_{\rm pd}$ with the matching condition given by Eq. (12), i.e., $k_p R_c = \gamma_g^{1/2}\left(u_2^2 - u_1^2\right)^{1/2}$ for $u_2 > u_1$ and the glass with the relative dielectric constant $\varepsilon_r = 2.25$. Hence, the damping of wakefields during the laser pulse propagation is dominated by the energy depletion of the laser pulse as given in Eq. (13). Thus, integrating the equations of motion in Eq. (11) over $\Psi_0 \leq \Psi \leq \Psi_{\rm mix}$, the energy $m_e c^2 \gamma$ and phase of the electron can be obtained as

$$\gamma(\Psi) = \gamma_0 + G(\Psi) - G(\Psi_0), \quad \Psi(z) = \Psi_0 + k_p z/\left(2\gamma_g^2\right), \tag{14}$$

where $m_e c^2 \gamma_0$ is the initial electron energy, Ψ_0 the initial electron phase with respect to the wakefield, $\Psi_{\rm mix} = \Psi(z_{\rm mix}) = \Psi_0 + \sqrt{2}\gamma_g$ the maximum electron phase in the wakefield for the matching condition in Eq. (12) and the laser pulse length $k_p c\tau = \sqrt{2}$, and

$$
\begin{aligned}
G(\Psi) = \gamma_g^2 \sqrt{\frac{\pi}{2}}a_0{}^2(C_1 + C_2)e^{-\left(1 + 4\alpha_d a_0^2\Psi\right)/2}\Bigg[&\frac{\sin\Psi - 2\alpha_d a_0^2 \cos\Psi}{1 + 4\alpha_d^2 a_0^4} \\
&- \frac{\sqrt{C_1 C_2}}{2(C_1 + C_2)}\left(\frac{\cos\delta}{\alpha_d a_0^2} - \frac{\sin(2\Psi + \delta) - \alpha_d a_0^2 \cos(2\Psi + \delta)}{1 + \alpha_d^2 a_0^4}\right)\Bigg].
\end{aligned}
\tag{15}
$$

The maximum energy gain to be attainable at $\Psi \to \infty$ is obtained as

$$
\begin{aligned}
\Delta\gamma_{\rm max}(\delta) &= \gamma_{\rm max} - \gamma_0 = G(\infty) - G(0) \\
&= \gamma_g^2 \sqrt{\frac{\pi}{2}}a_0{}^2(C_1 + C_2)e^{-1/2}\left[\frac{2\alpha_d a_0^2}{1 + 4\alpha_d^2 a_0^4} + \frac{\sqrt{C_1 C_2}}{2(C_1 + C_2)}\left(\frac{\cos\delta}{\alpha_d a_0^2} - \frac{\sin\delta - \alpha_d a_0^2 \cos\delta}{1 + \alpha_d^2 a_0^4}\right)\right].
\end{aligned}
\tag{16}
$$

Considering the mixing of two lowest order hybrid modes EH_{11} and EH_{12} with the coupling efficiencies $C_1 = 0.4022$ and $C_2 = 0.4986$, the evolution of the energy gain with respect to γ_g^2 is shown in **Figure 2a** for various detuning phases δ in comparison with that of the EH_{11} monomode with $C_1 = 1$ and $C_2 = 0$. The effect of phase mismatching on the maximum attainable energy gain is shown in **Figure 2b** for various normalized laser intensities a_0^2 in the quasi-linear regime. One can see that the growth of energy gain occurs in the relatively wide range of the phase mismatching over $-\pi/2 \leq \delta \leq \pi/2$ and that the maximum attainable energy gain does not strongly depend on the normalized vector potential a_0 in the quasi-linear regime. While the single-mode LPA driven by the normalized intensity $a_0^2 = 1$ reaches the maximum energy gain $\Delta\gamma_{\rm max} = 0.71\gamma_g^2$ over the accelerating phase
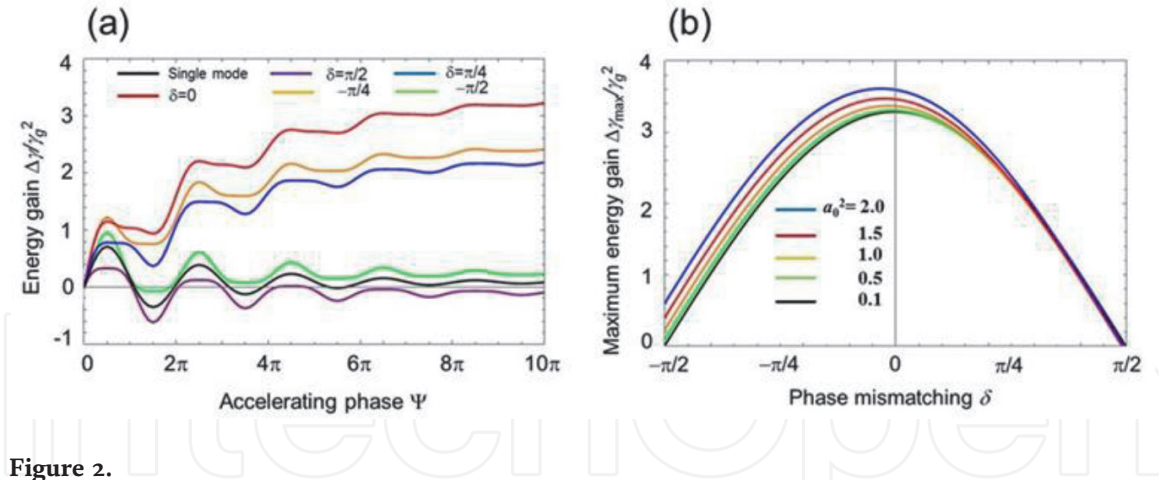
Figure 2.
(a) The evolution of the energy gain normalized to γ_g^2 of the mode mixing LPA comprising two hybrid modes EH_{11} and EH_{12} coupled to the airy beam intensity of $a_0^2 = 1$ with the coupling efficiency $C_1 = 0.4022$ and $C_2 = 0.4986$, respectively, as a parameter of the mismatching phase δ. The black curve shows that for the single-mode LPA with $C_1 = 1$ and $C_2 = 0$. (b) The maximum attainable energy gain of the two-mode mixing LPA for various normalized intensities a_0^2 as a function of the phase mismatching.

$0 \leq \Psi \leq \pi/2$, the two-mode mixing LPA with the phase matching, i.e., $\delta = 0$, is attainable to the maximum energy gain $\Delta\gamma_{\max} = 3.2\gamma_g^2$ over the accelerating phase region $\Delta\Psi = 10\pi$, as shown in **Figure 2**. It is noted that significant enhancement of the energy gain is attributed to a large energy transfer efficiency from the laser pulse to the wakefield, i.e., $\eta_{\text{laser}\rightarrow\text{wake}} \sim 96\%$ over the accelerating phase region $\Delta\Psi = 10\pi$, while the energy transfer efficiency for the single-mode LPA is $\eta_{\text{laser}\rightarrow\text{wake}} \sim 17\%$ over the accelerating phase region $\Delta\Psi = \pi/2$.

The average energy gain of electrons contained in the bunch with the root-mean-square (rms) bunch length $k_p\sigma_z$ and longitudinal Gaussian density distribution $\rho_\|(\Psi') = e^{-\Psi'^2/2k_p^2\sigma_z^2}/(\sqrt{2\pi}k_p\sigma_z)$ can be estimated as $\langle\Delta\gamma\rangle = \langle G(\Psi)\rangle - \langle G(\Psi_0)\rangle$, where

$$\langle G(\Psi)\rangle = \int_{-\infty}^{\infty}\rho_\|(\Psi' - \Psi)G(\Psi')d\Psi' \approx \sqrt{\frac{\pi}{2}}a_0^2\gamma_g^2(C_1 + C_2)e^{-(1+4\alpha_d a_0^2\Psi)/2}$$

$$\times\left[\frac{e^{-k_p^2\sigma_z^2/2}\left(\sin\Psi - 2\alpha_d a_0^2\cos\Psi\right)}{1 + 4\alpha_d^2 a_0^4} - \frac{\sqrt{C_1 C_2}}{2(C_1 + C_2)}\left(\frac{1}{\alpha_d a_0^2} - \frac{e^{-2k_p^2\sigma_z^2}\left(\sin 2\Psi - \alpha_d a_0^2\cos 2\Psi\right)}{1 + \alpha_d^2 a_0^4}\right)\right].$$

$$(17)$$

Figure 3 shows the evolution of the energy gain and the maximum attainable energy gain averaged over electrons in a Gaussian bunch with various rms lengths. It is noted that the maximum attainable energy gain at $\Psi \rightarrow \infty$ exhibits weak dependence on the initial bunch phase Ψ_0 for a long bunch and that the minimum energy spread occurs at $\Psi_0 \sim 0$ for different bunch lengths.

3.2 Beam loading

In the linear regime, a solution of the Green's function for the beam-driven wakefield excited by a charge bunch with bi-Gaussian density distribution $\rho_b = \rho_\|(\xi)\rho_\perp(r)$, i.e., $\rho_\|(\xi) = qn_b\exp\left(-\xi^2/2\sigma_z^2\right)$ and $\rho_\perp(r) = \exp\left(-r^2/2\sigma_r^2\right)$ for the rms bunch length σ_z, rms bunch radius σ_r, and particle charge q (+e for a positron beam and −e for an electron beam), is written as $E_{zb}(r,\xi) = Z(\xi)R(r)$, where $\xi = z - ct$ is the coordinate in the co-moving frame of a relativistic electron beam with $v_z \simeq c$ and r is the radial, transverse coordinate of an electron beam having a cylindrical symmetry [38]. Here, the longitudinal and transverse plasma responses are obtained as
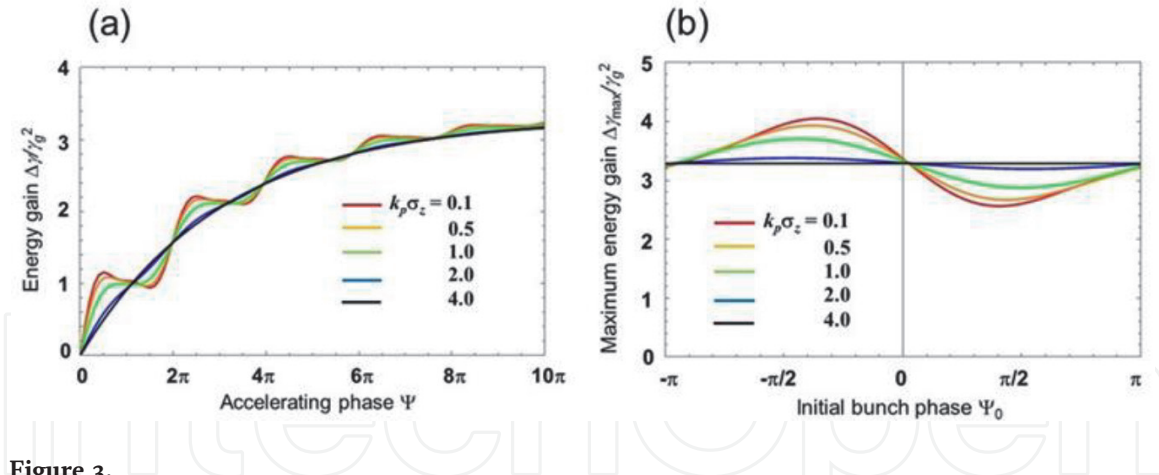
Figure 3.
*(a) The evolution of the energy gain $\Delta\gamma/\gamma_g^2$ of the mode mixing LPA driven by two hybrid modes EH_{11} and EH_{12} with the same parameters as those of **Figure 2a** for various rms bunch lengths $k_p\sigma_z$. (b) The maximum attainable energy gain of two-mode mixing LPA for various rms bunch lengths as a function of the initial phase of the bunch center with respect to the maximum accelerating field.*

$$Z(\xi) = -4\pi \int_\xi^\infty d\xi' \rho_\|(\xi') \cos k_p(\xi - \xi') = -(2\pi)^{3/2} q n_b \sigma_z e^{-k_p^2\sigma_z^2/2}$$
$$\times \left[\cos k_p\xi \left(1 - \Re\mathrm{erf}\frac{\xi/\sigma_z + ik_p\sigma_z}{\sqrt{2}}\right) + \sin k_p\xi\, \Im\mathrm{erf}\frac{\xi/\sigma_z + ik_p\sigma_z}{\sqrt{2}} \right], \tag{18}$$

and inside the bunch $(r < r')$

$$R(r) = \left(k_p^2/2\pi\right) \int_0^{2\pi} d\theta \int_0^\infty r'dr' \rho_\perp(r') K_0\left(k_p\left|\vec{r} - \vec{r'}\right|\right)$$
$$= \left(k_p^2\sigma_r^2/2\right) e^{k_p^2\sigma_r^2/2} \Gamma\left(0, k_p^2\sigma_r^2/2\right) J_0\left(k_pr\right), \tag{19}$$

where K_0 is the modified Bessel function of the second kind and $\Gamma(\alpha, x) = \int_x^\infty e^{-t} t^{\alpha-1} dt$ is the incomplete Gamma function of the second kind. Combining the longitudinal and transverse solutions, the wakefield excited by a bi-Gaussian-shaped bunch is obtained as

$$E_{zb}(r, \xi)/E_0 = -(q/e)k_p r_e N_b \Theta_G(\sigma_r, \sigma_z) J_0\left(k_pr\right)$$
$$\times \left[\cos k_p\xi \left(1 - \Re\mathrm{erf}\frac{\xi/\sigma_z + ik_p\sigma_z}{\sqrt{2}}\right) + \sin k_p\xi\, \Im\mathrm{erf}\frac{\xi/\sigma_z + ik_p\sigma_z}{\sqrt{2}} \right], \tag{20}$$

where $r_e = e^2/m_e c^2$ is the electron classical radius, $N_b = (2\pi)^{3/2}\sigma_r^2\sigma_z n_b$ the number of particles in a bunch, and $\Theta_G(\sigma_r, \sigma_z) \equiv e^{-k_p^2\sigma_z^2/2} e^{k_p^2\sigma_r^2/2} \Gamma\left(0, k_p^2\sigma_r^2/2\right)$. If we consider a laser-driven wakefield E_{zL} excited by two mixing hybrid modes accelerating the electron beam in a gas-filled capillary, the net longitudinal electric field, i.e., the beam loading field, experienced by the electron beam is given by $E_{zBL} = E_{zL} + E_{zb}$. From Eqs. (13) and (20), the beam loading field at $r = 0$ consisting of the laser- and beam-driven wake, where the electron bunch is located at $\Psi = \Psi_b$ in the laser co-moving frame, i.e., $k_p\xi \approx \Psi - \Psi_b$, yields

$$E_{zBL}(0, \Psi)/E_0 = \hat{E}_{zL}(\Psi)\cos\Psi + k_p r_e N_b \Theta_G(\sigma_r, \sigma_z)$$
$$\times \left[\cos(\Psi - \Psi_b)\Re\mathrm{erfc}\left(\frac{\Psi - \Psi_b}{\sqrt{2}k_p\sigma_z} + i\frac{k_p\sigma_z}{\sqrt{2}}\right) + \sin(\Psi - \Psi_b)\Im\mathrm{erf}\left(\frac{\Psi - \Psi_b}{\sqrt{2}k_p\sigma_z} + i\frac{k_p\sigma_z}{\sqrt{2}}\right) \right],$$
$$\tag{21}$$

where $\hat{E}_{zL}(\Psi) = -\sqrt{\pi/8}a_0{}^2e^{-(1+4\alpha_d a_0^2\Psi)/2}(C_1 + C_2 + \sqrt{C_1C_2}\cos\Psi)$. A loss of the energy gain due to the beam wakefield $E_{zb} = k_p r_e N_b \Theta_G(\sigma_r, \sigma_z)$ at the bunch center is

$$\Delta\gamma_{BL} = -\left(2\gamma_g^2/E_0\right)\int_{\Psi_0}^{\Psi} E_{zb}(\Psi')d\Psi' = -2\gamma_g^2\Theta_G(\sigma_r, \sigma_z)(\Psi - \Psi_0), \tag{22}$$

and the rms energy spread due to the beam loading is estimated as

$$\sigma_{\Delta\gamma_{BL}} \approx 2^{1/4}\gamma_g^2 k_p r_e N_b e^{k_p^2\sigma_r^2/2}\Gamma\left(0, k_p^2\sigma_r^2/2\right)S(k_p\sigma_z)(\Psi - \Psi_0), \tag{23}$$

where $S(k_p\sigma_z) = \left|(2/\pi)^{1/2} - k_p\sigma_z e^{-k_p^2\sigma_z^2/2}\mathrm{erf}(k_p\sigma_z/\sqrt{2})\right|$ has the minimum $S = 0.35$ at $k_p\sigma_z = 1.26$.

3.3 Betatron motion

In the wakefield, an electron moving along the z-axis undergoes a transverse focusing force $F_\perp^B = -m_e c^2 F_r x/r$ at the transverse displacement x and exhibits the betatron motion. Taking into account $F_r \approx (\partial F_r/\partial r)r$ near the z-axis $r \approx 0$, the focusing force is written by $F_\perp^B/m_e c^2 = -(\partial F_r/\partial r)x = -K^2 x$, where $K = (\partial F_r/\partial r)^{1/2}$ is the focusing constant. For the optimum pulse length of $k_p c\tau = \sqrt{2}$ and $\Psi = k_p z/\left(2\gamma_g^2\right) \gg k_p c\tau/\left(2\gamma_g^2\right) = 1/\left(\sqrt{2}\gamma_g^2\right)$ in Eq. (8), transverse laser wakefield in the matching condition $\Delta k_{z12} \approx \left(u_2^2 - u_1^2\right)/\left(k_0 R_c^2\right) = k_p/\gamma_g^2$ is given by

$$\begin{aligned}
\frac{F_{rL}}{E_0} &= \sqrt{\frac{\pi}{2}}\frac{a_0^2 e^{-1/2}}{\sqrt{\gamma_g\left(u_2^2 - u_1^2\right)}}\left[\left(C_1 u_1 J_0\left(\frac{u_1 r}{R_c}\right)J_1\left(\frac{u_1 r}{R_c}\right) + C_2 u_2 J_0\left(\frac{u_2 r}{R_c}\right)J_1\left(\frac{u_2 r}{R_c}\right)\right)\sin\Psi \right. \\
&\left. + \frac{\sqrt{C_1C_2}}{2}\left(u_1 J_0\left(\frac{u_2 r}{R_c}\right)J_1\left(\frac{u_1 r}{R_c}\right) + u_2 J_0\left(\frac{u_1 r}{R_c}\right)J_1\left(\frac{u_2 r}{R_c}\right)\right)\sin 2\Psi\right].
\end{aligned} \tag{24}$$

Transverse wakefield excited by the electron bunch is obtained from Eq. (20) according to the Panofsky-Wenzel theorem [39], $\partial E_z/\partial r = \partial(E_r - B_\theta)/\partial\xi$, leading to the beam focusing force [40].

$$\begin{aligned}
F_{rb}(r, \xi)/E_0 &= (E_r - B_\theta)/E_0 = (q/e)k_p r_e N_b \Theta_G(\sigma_r, \sigma_z)J_1(k_p r) \\
&\times\left[\sin k_p\xi\left(1 - \Re\mathrm{erf}\frac{\xi/\sigma_z + ik_p\sigma_z}{\sqrt{2}}\right) - \cos k_p\xi\,\Im\mathrm{erf}\frac{\xi/\sigma_z + ik_p\sigma_z}{\sqrt{2}}\right].
\end{aligned} \tag{25}$$

At the bunch center $\xi = 0$, the on-axis beam focusing strength at $r = 0$

$$\frac{\partial F_{rb}}{E_0 k_p \partial r} = \frac{k_p r_e N_b}{\sqrt{\pi}}e^{k_p^2\sigma_r^2/2}\Gamma\left(0, \frac{k_p^2\sigma_r^2}{2}\right)\mathrm{F}\left(\frac{k_p\sigma_z}{\sqrt{2}}\right), \tag{26}$$

where $\mathrm{erf}(ik_p\sigma_z/\sqrt{2}) = (2i/\sqrt{\pi})\int_0^{k_p\sigma_z/\sqrt{2}}e^{z^2}dz = (2i/\sqrt{\pi})e^{\frac{k_p^2\sigma_z^2}{2}}\mathrm{F}(k_p\sigma_z/\sqrt{2})$ and $\mathrm{F}(x) = e^{-x^2}\int_0^x e^{z^2}dz$ is Dawson's integral. Near-axis electrons experience the normalized accelerating and focusing gradients at $r = 0$, as obtained from Eqs. (21), (24), and (26)

$$\frac{E_{z\mathrm{BL}}}{E_0} = -\frac{1}{2}\sqrt{\frac{\pi}{2}}a_0^2 e^{-(1+4\alpha a_0^2\Psi)/2}(C_1+C_2)\left[\cos\Psi + \frac{\sqrt{C_1C_2}}{C_1+C_2}(1+\cos 2\Psi)\right]$$
$$+ k_p r_e N_b \Theta_G(\sigma_r,\sigma_z), \tag{27}$$

and

$$\frac{\partial F_{r\mathrm{BL}}}{E_0 k_p \partial r} = -\frac{1}{2}\sqrt{\frac{\pi}{2}}a_0^2 e^{-(1+4\alpha a_0^2\Psi)/2}\frac{u_1^2 C_1 + u_2^2 C_2}{\gamma_g(u_2^2-u_1^2)}\left[\sin\Psi + \frac{(u_1^2+u_2^2)\sqrt{C_1C_2}}{2(u_1^2 C_1 + u_2^2 C_2)}\sin 2\Psi\right]$$
$$+ \frac{k_p r_e N_b}{\sqrt{\pi}}\Theta_F(\sigma_r,\sigma_z), \tag{28}$$

where $\Theta_F(\sigma_r,\sigma_z) \equiv e^{k_p^2\sigma_r^2/2}\Gamma\left(0,k_p^2\sigma_r^2/2\right)\mathrm{F}\left(k_p\sigma_z/\sqrt{2}\right)$ is the bunch form factor for a bi-Gaussian profile with the rms bunch radius σ_r and length σ_z.

The equations of motion of an electron propagating in the wakefield behind the laser pulse is written as [41].

$$\frac{d^2\bar{x}}{d\bar{t}^2} - \frac{\bar{E}_z}{\gamma}\frac{d\bar{x}}{d\bar{t}} + \frac{\bar{K}^2}{\gamma}\bar{x} = 0, \quad \frac{d\gamma}{d\bar{t}} = -\bar{E}_z, \tag{29}$$

where $\bar{x} = k_p x$ and $\bar{t} = \omega_p t$ are the normalized variables of x and t, respectively. Here the longitudinal wakefield and focusing constant at $r = 0$ are defined as $\bar{E}_z \equiv E_{z\mathrm{BL}}/E_0$ and $\bar{K}^2 \equiv (1/E_0 k_p)(\partial F_{r\mathrm{BL}}/\partial r)$, respectively. If one can assume that $\bar{E}_z$ and $\bar{K}$ are constant along the particle trajectory, introducing a new variable $s = \left(4\gamma\bar{K}^2/\bar{E}_z^2\right)^{1/2}$ to obtain the differential equation $s\left(d^2\bar{x}/ds^2\right) + (d\bar{x}/ds) + s\bar{x} = 0$, general solutions of which are the Bessel functions of the first kind $J_0(s)$ and the second kind $Y_0(s)$, the solutions of the coupled equations are given by Eqs. (14) and (15) for γ, and the transverse position and velocity [41].

$$\begin{pmatrix} \bar{x}(s) \\ \beta_x(s) \end{pmatrix} = \mathbf{M}(s|s_0)\begin{pmatrix} \bar{x}_0(s_0) \\ \beta_{x0}(s_0) \end{pmatrix}, \tag{30}$$

where $\beta_x = \beta_g(d\bar{x}/d\bar{t})$, subscripts "0" denote the initial values, and

$$\mathbf{M}(s|s_0) = \begin{pmatrix} \dfrac{\pi}{2}s_0[J_1(s_0)Y_0(s) - Y_1(s_0)J_0(s)] & \dfrac{\pi\gamma_0}{E_{z0}}[J_0(s)Y_0(s_0) - Y_0(s)J_0(s_0)] \\ -\dfrac{\pi E_z s_0 s}{4\gamma}[J_1(s)Y_1(s_0) - Y_1(s)J_1(s_0)] & \dfrac{\pi E_z}{2E_{z0}}\dfrac{\gamma_0}{\gamma}s[J_1(s)Y_0(s_0) - Y_1(s)J_0(s_0)] \end{pmatrix}. \tag{31}$$

While the electron stays in the focusing region of the wakefield, i.e., $\partial F_r/\partial r > 0$, the electron exhibits betatron oscillation at the frequency given by $\omega_\beta = ds/dt = \omega_p \bar{K}/\gamma^{1/2}$. Contrarily, when the electron moves to the defocusing region where $\partial F_r/\partial r < 0$ and s becomes imaginary, the amplitude of the electron trajectory increases monotonically as a result of the Bessel functions being transformed to the modified Bessel functions, leading to ejection of the electron from the wakefield [41]. Hence, the requirement of betatron oscillation in the focusing region $\bar{K}^2 > 0$

demands that the minimum number of electrons contained in a bunch should be injected into the plasma as given by

$$N_b \geq \frac{\sqrt{\pi}}{k_p r_e \Theta_F(\sigma_r, \sigma_z)} \left| \frac{\partial F_{rL}(\Psi)}{E_0 k_p \partial r} \right|_{\max},$$ (32)

for a bi-Gaussian bunch with the rms radius σ_r and length σ_z. **Figure 4** shows a map of the bunch form factor $\Theta_F(\sigma_r, \sigma_z)$ and the minimum number of electrons contained in a bunch requisite for the beam self-focusing strength larger than the defocusing strength in the laser-driven wakefield for the EH_{11}-EH_{12} mode mixing LPA. It is noted that the minimum value of the requisite electron number occurs at the bunch length $k_p \sigma_z = 1.31$ for various bunch radii, e.g., $N_b \geq 3.63 \times 10^7$ for $k_p \sigma_r = 1$ and $N_b \geq 7.05 \times 10^6$ for $k_p \sigma_r = 0.1$, as shown in **Figure 4**.

In the bunch containing the requisite number of particles, an electron undergoes betatron motion throughout the whole accelerating phase, as shown in **Figure 5**, where the trajectory and momentum of the electron in the bunch with the number of electrons $N_b = 1 \times 10^8$ and length $k_p \sigma_z = 1.3$ are calculated from Eq. (30) in 10^5 segments of the laser wakefield phase excited in the plasma with density $n_e = 1 \times 10^{18}$ cm^{-3}. Note that the betatron oscillation exhibits beats with the amplitude modulation due to the accelerating wakefield.

3.4 Effects of radiation reaction and multiple Coulomb scattering

A beam electron propagating in the wakefield undergoes betatron motion that induces synchrotron (betatron) radiation at high energies. The synchrotron radiation causes the radiation damping of particles and affects the energy spread and transverse emittance via the radiation reaction force. Furthermore, a notable difference of plasma-based accelerators from vacuum-based accelerators is the presence of the multiple Coulomb scattering between beam electrons and plasma ions, which counteracts the beam focusing due to the transverse wakefield and radiation damping due to betatron radiation. The comprehensive motion of an electron traveling along the z-axis is described as
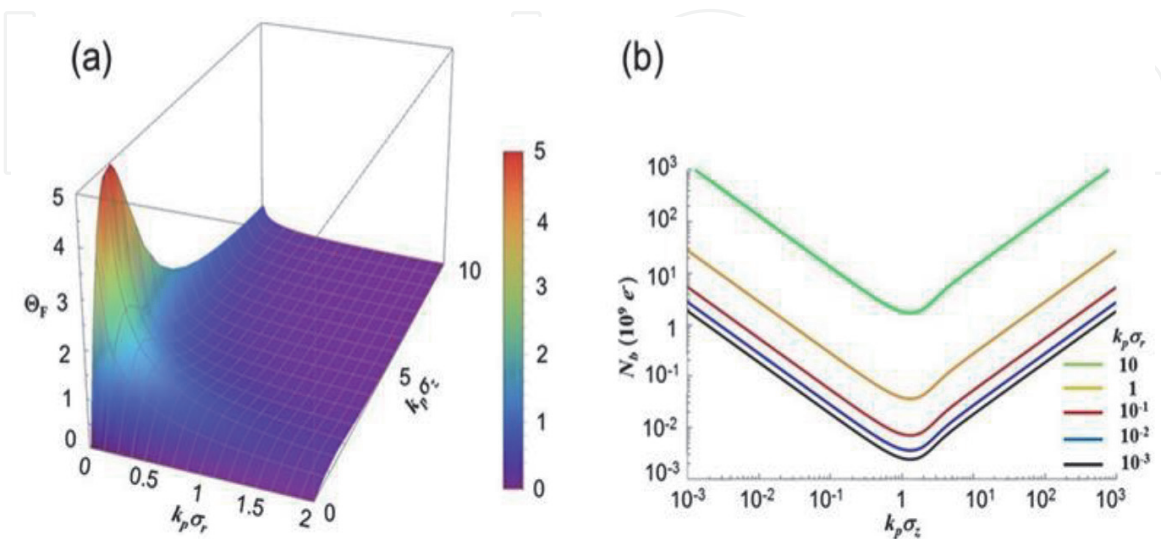

Figure 4.
(a) A map of the bunch form factor $\Theta_F(\sigma_r, \sigma_z)$ for the beam self-focusing strength of a bi-Gaussian bunch as a function of the dimensionless rms bunch radius $k_p \sigma_r$ and length $k_p \sigma_z$. (b) The minimum number of electrons contained in a Gaussian bunch requisite for the beam self-focusing strength larger than the defocusing strength from the laser-driven wakefield in the EH_{11}-EH_{12} mode mixing LPA.
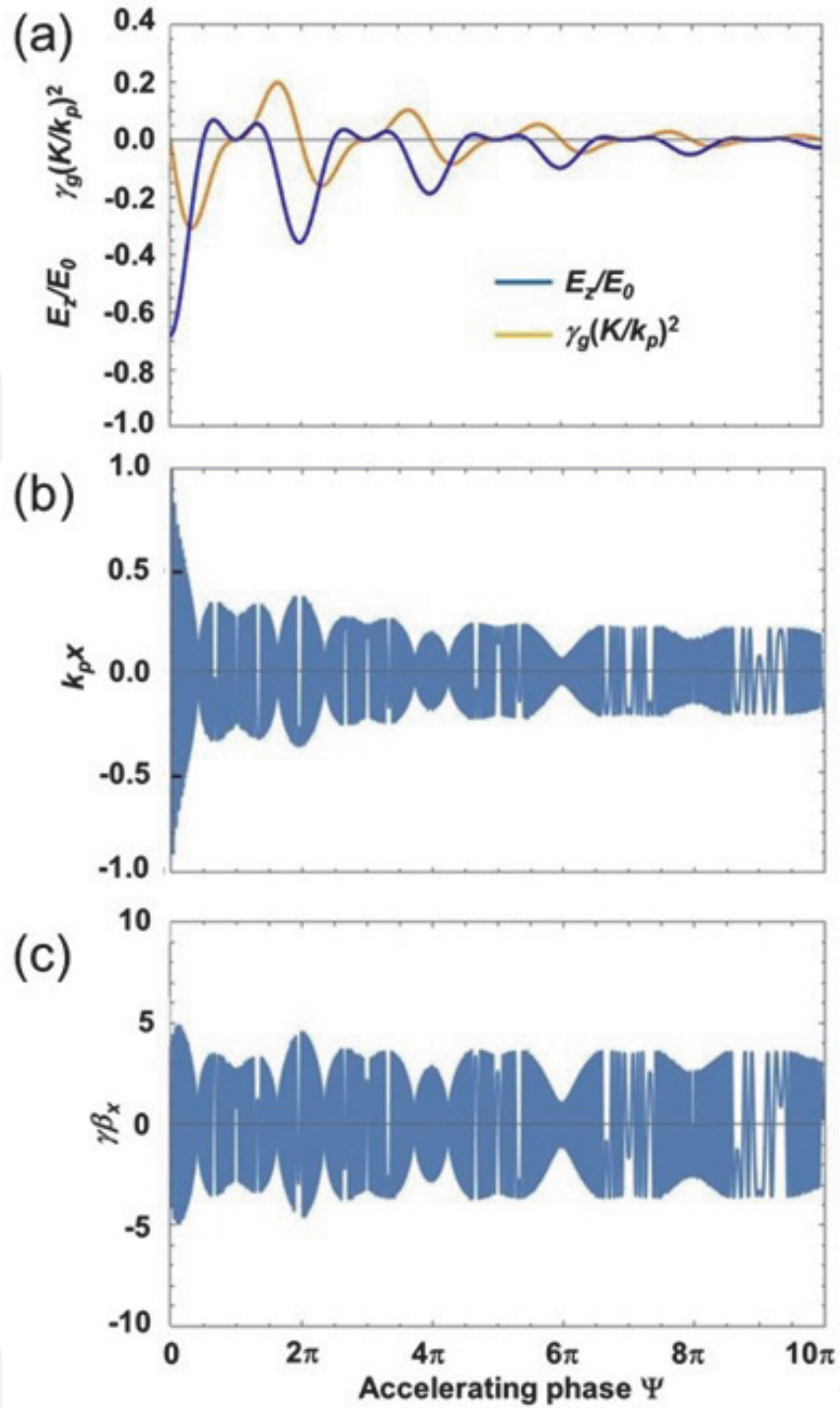
Figure 5.
*(a) Normalized accelerating wakefield E_z/E_0 and focusing strength $\gamma_g K^2/k_p^2 = \gamma_g(1/E_0 k_p)(\partial F_{rL}/\partial r)$ in the EH_{11}-EH_{12} mode mixing LPA with the same parameters as those of **Figure 2a** as a function of the accelerating phase Ψ. (b and c) normalized trajectory $k_p x$ and transverse momentum $\gamma\beta_x$ of the electron with the initial values $m_e c^2 \gamma_0 = 100\,MeV$, $k_p x_0 = 1$, and $\gamma\beta_{x0} = 0$ in the bunch with the number of electrons $N_b = 1 \times 10^8$ and length $k_p \sigma_z = 1.3$ for betatron motion in the laser wakefields (a) with electron density $n_e = 1 \times 10^{18}\,cm^{-3}$.*

$$\frac{du_x}{cdt} = \frac{F_\perp^B}{m_e c^2} + \frac{F_x^R}{m_e c^2} + \frac{du_x^S}{cdt}, \frac{du_z}{cdt} = -k_p \frac{E_z}{E_0} + \frac{F_z^R}{m_e c^2}, \tag{33}$$

where $\mathbf{u} = \mathbf{p}/m_e c$ is the normalized electron momentum, $\mathbf{F}^R$ the radiation reaction force, and $u_x^S \approx \gamma\theta_x$ the transverse kick in momentum projected onto the x-plane due to multiple Coulomb scattering through small deflection angles θ.

For the classical expression of the radiation reaction force given by [42].

$$\frac{\mathbf{F}^{\mathrm{R}}}{m_e c \tau_R} = \frac{d}{dt}\left(\gamma \frac{d\mathbf{u}}{dt}\right) + \gamma \mathbf{u}\left[\left(\frac{d\gamma}{dt}\right)^2 - \left(\frac{d\mathbf{u}}{dt}\right)^2\right], \qquad (34)$$

where $\gamma = (1 + u^2)$ is the relativistic Lorentz factor of the electron and $\tau_R = 2r_e/3c \simeq 6.26 \times 10^{-24}$s, assuming $u_z \gg u_x$ and $dx/dt = cu_x/\gamma \simeq cu_x/u_z$, the radiation reaction force Eq. (34) is approximately read as [43].

$$F_x^{\mathrm{R}}/(m_e c^2) \simeq -c\tau_R K^2 u_x(1 + K^2\gamma x^2), F_z^{\mathrm{R}}/(m_e c^2) \simeq -c\tau_R K^4 \gamma^2 x^2. \qquad (35)$$

Since the scale length of the radiation reaction, i.e., $c\tau_R = 2r_e/3 \simeq 1.9$ fm, is much smaller than that of the betatron motion, i.e., $\sim \lambda_p\sqrt{\gamma}$, the radiation reaction force is considered as a perturbation in the betatron motion.

A beam electron of the incident momentum $p = \gamma m_e v$, passing a nucleus of charge Ze at impact parameter b in the plasma, suffers an angular deflection $\theta = \Delta p/p \simeq 2e^2 Z/(pbv)$ due to Coulomb scattering [44]. The successive collisions of the relativistic beam electrons with $v \sim c$ while traversing the plasma of ion density $n_i = n_e/Z$ results in an increase of the mean square deflection angle at a rate [8, 44].

$$\frac{d\langle\theta^2\rangle}{cdt} = \frac{8\pi n_i Z^2 r_e^2}{\gamma^2}\ln\left(\frac{b_{\max}}{b_{\min}}\right) = \frac{2k_p^2 r_e Z}{\gamma^2}\ln\left(\frac{\lambda_D}{R_N}\right), \qquad (36)$$

where $b_{\max} = \lambda_D = (T_e/4\pi n_e e^2)^{1/2}$ is the plasma Debye length at the temperature T_e and $R_N \approx 1.4 A^{1/3}$ fm is the effective Coulomb radius of the nucleus with the mass number A. Here, the logarithm $\ln(b_{\max}/b_{\min})$ is approximated as $\ln(\lambda_D/R_N) \approx 24.7\left[1 + 0.047\log\left(n_e T_e A^{2/3}\right)\right]$ for n_e [10^{16} cm^{-3}] and T_e [eV] [45]. The multiple-scattering distribution for the projected angle θ_x is approximately Gaussian for small deflection angles, given by the probability distribution function $P(\theta_x) = 1/(\pi\langle\theta^2\rangle)^{1/2}\exp\left(-\theta_x^2/\langle\theta^2\rangle\right)$. Thus, the transverse momentum $u_x^{\mathrm{S}} \approx \gamma\theta_x$ is obtained from using the normal distribution with the standard deviation $(\langle\theta^2\rangle/2)^{1/2}$ around the mean angle 0 at the successive time step along the particle trajectory.

The electron orbit and energy are obtained from the solutions of the coupled equations in Eq. (33) describing the single particle motion in the segmented phase, where $\overline{E}_z$ and $\overline{K}$ are assumed to be constant over the phase advance $\Delta\Psi$. Provided the initial values of $\overline{x}_0$ and β_{x0} are specified from the energy γ_0, relative energy spread $\Delta\gamma/\gamma_0$, and normalized emittance ε_{n0} of the injected beam, $\gamma(s)$, $\overline{x}(s)$, and $\beta_x(s)$ are first calculated from Eqs. (14) and (30) using $s(\Psi)$, where $\Psi = \Psi_0 + \Delta\Psi$ is the phase at next step. Thus, the effects of the radiation reaction and multiple Coulomb scattering are obtained as follows:

$$\beta_x(s) = \beta_x^{\mathrm{B}}(s) + \Delta\beta_x^{\mathrm{R}}(s_0) + \Delta\beta_x^{\mathrm{S}}(s_0), \ \gamma(\Psi) = \gamma^{\mathrm{A}}(\Psi) + \Delta\gamma^{\mathrm{R}}(\Psi_0), \qquad (37)$$

where $\beta_x^{\mathrm{B}}(s)$ and $\gamma^{\mathrm{A}}(\Psi)$ are the solutions obtained from Eqs. (30) and (14), respectively; $\Delta\beta_x^{\mathrm{R}}(s_0)$ and $\Delta\gamma^{\mathrm{R}}(\Psi_0)$ are correction terms for the effect of the radiation reaction force, given by

$$\Delta\beta_x^{\mathrm{R}} = -2C_R\gamma_g\beta_{x0}\overline{K}_0^2\left(1 + \gamma_0\overline{K}_0^2\overline{x}_0^2\right)\Delta\Psi, \ \Delta\gamma^{\mathrm{R}}(\Psi_0) = -2C_R\gamma_g\gamma_0^2\overline{K}_0^2\overline{x}_0^2\Delta\Psi, \qquad (38)$$

with $C_R = k_p c \tau_R \gamma_g = (2/3) k_p r_e \gamma_g = 11.8 \times 10^{-9} [\mu m]/\lambda_0$ and $\overline{K}_0^2 = \overline{K}^2(\Psi_0)$; and $\Delta \beta_x^S(s_0) = \theta_x$ is a projected angle due to multiple Coulomb scattering, the standard deviation of which is obtained from Eq. (36) for $\lambda_0 = 1$ μm as

$$\sigma_{\theta_x} = \sqrt{\langle \theta^2 \rangle / 2} \approx 2.66 \times 10^{-4} \left[\gamma_g \Delta \Psi \ln(\lambda_D/R_N) \right]^{1/2} / \gamma_0. \tag{39}$$

The radiated power of the electron in the classical limit is given by [42, 43].

$$P_{\text{rad}} = \frac{2e^2 \gamma^2}{3c} \left[\left(\frac{d\mathbf{u}}{dt} \right)^2 - \left(\frac{d\gamma}{dt} \right)^2 \right] = \frac{2e^2 \gamma^2}{3m_e^2 c^3} \left[|\mathbf{F}_{\text{ext}}|^2 - |\mathbf{F}_{\text{ext}} \cdot \mathbf{u}/\gamma|^2 \right]. \tag{40}$$

where $\mathbf{F}_{\text{ext}}$ is the external force and $m_e c d\gamma/dt = \mathbf{F}_{\text{ext}} \cdot \mathbf{u}/\gamma$ is used. For a relativistic electron with $u_x^2 \ll \gamma^2$ and $u_z \sim \gamma$, taking into account $\mathbf{F}_{\text{ext}} = F_\perp \mathbf{e}_x + F_\parallel \mathbf{e}_z$ with $F_\perp = -m_e c^2 K^2 x$ and $F_\parallel = -eE_z$, the radiated power can be written as $P_{\text{rad}} = 2e^2 \gamma^2 F_\perp^2/(3m^2 c^3) = mc^4 \tau_R \gamma^2 K^4 x^2$, which means the radiative damping rate $\nu_R = P_{\text{rad}}/(\gamma m_e c^2) = \tau_R c^2 \gamma K^4 x^2$. Thus, a total radiation energy loss along the particle orbit is estimated as

$$\Delta \gamma_{\text{rad}} = \frac{1}{m_e c^2} \int_{t_0}^{t} dt P_{\text{rad}}(t) = \sum |\Delta \gamma^R(\Psi_0)|. \tag{41}$$

3.5 Numerical studies of the single-particle dynamics in a single stage

Numerical calculations of the single-particle dynamics can be carried out throughout the segments in phase Ψ for a set of test particles under the initial conditions, and then the underlying beam parameters can be obtained as an ensemble average over test particles: for instance, the mean energy is calculated as $\langle \gamma \rangle = \sum_i \gamma_i / N_p$, where γ_i is the energy of the i-th particle and N_p the number of test particles, and the energy spread is defined as $\sigma_\gamma = \left(\langle \gamma^2 \rangle - \langle \gamma \rangle^2 \right)^{1/2}$. The normalized transverse emittance is obtained from

$$\varepsilon_n = \left[\left\langle (x - \langle x \rangle)^2 \right\rangle \left\langle (u_x - \langle u_x \rangle)^2 \right\rangle - \langle (x - \langle x \rangle)(u_x - \langle u_x \rangle) \rangle^2 \right]^{1/2}, \tag{42}$$

where $u_x = \gamma \beta_x$ is the dimensionless transverse momentum.

The particle orbit and energy can be numerically tracked by using the solutions of the single particle motion (Eqs. (30) and (14)) associated with the perturbation arising from the effects of the radiation reaction and multiple Coulomb scattering, as given by Eqs. (38) and (39), respectively. The simulation of particle tracking can be carried out by using an ensemble of 10^4 test particles, for which the initial values at the injection and the deflection angles due to the multiple Coulomb scattering at each segment in a phase step $\Delta \Psi/400$, where $\Delta \Psi = 10\pi$ is the phase advance in the single stage, are obtained from the random number generator for the normal distribution, assuming that the particle beam with the rms bunch length $\sigma_z = 16$ μm ($k_p \sigma_z = 3$) containing $N_b = 1 \times 10^8$ electrons (16 pC) is injected into the capillary accelerator operated at the plasma density of $n_e = 1 \times 10^{18}$ cm^{-3} from the external injector at the injection energy $E_{\text{inj}} = m_e c^2 \gamma_0$ and the initial normalized transverse emittance ε_{n0} in the condition initially matched to laser wakefields, namely, the initial bunch radius $\overline{x}_0 = k_p \sigma_0 = (k_p \varepsilon_{n0})^{1/2} / \left(\gamma_0 \overline{K}^2 \right)^{1/4}$ and momentum $\gamma_0 \beta_0 =$
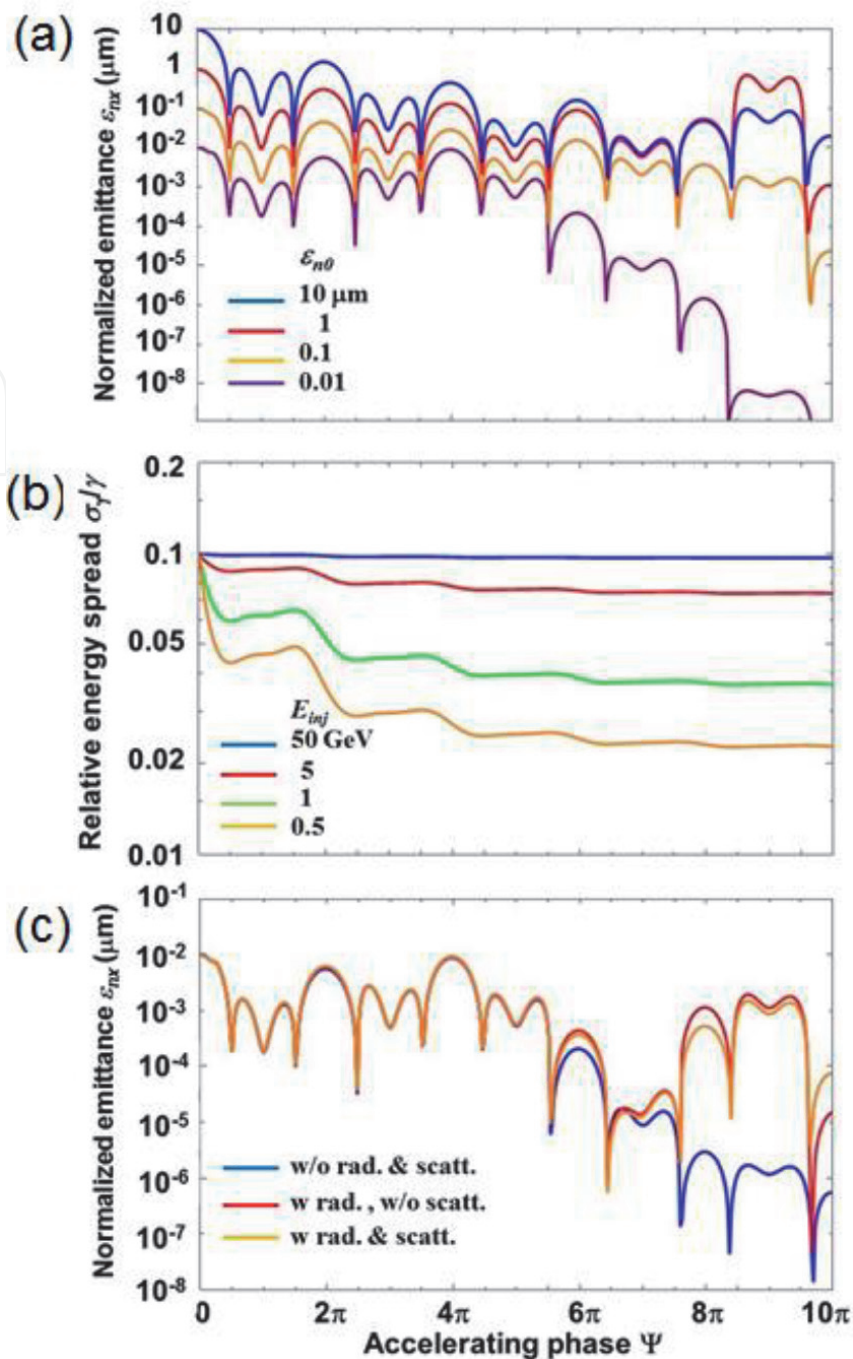
Figure 6.
*Numerical results of the beam dynamics study on the two-mode mixing single-stage LPA (**Figure 1a**) at the plasma density $n_e = 1 \times 10^{18}$ cm^{-3} and number of electrons $N_b = 1 \times 10^8$ in a bunch with length $k_p \sigma_z = 3$. (a) Evolution of transverse normalized emittance ε_{nx} from various initial values for the initial energy $E_{inj} = m_e c^2 \gamma_0 = 1$ GeV and relative energy spread $\sigma_\gamma/\gamma_0 = 0.1$ without radiation and multiple Coulomb scattering. (b) Evolution of relative energy spread σ_γ/γ from the initial value of 0.1 for various initial energies E_{inj} due to radiation reaction without multiple Coulomb scattering. (c) Evolution of transverse normalized emittance from the initial value $\varepsilon_{n0} = 0.01$ μm for various cases with and without the radiation reaction and multiple Coulomb scattering.*

$\left(\gamma_0 \overline{K}^2\right)^{1/4} \left(k_p \varepsilon_{n0}\right)^{1/2}$ with the focusing strength $\overline{K}^2$, given by Eq. (28). **Figure 6a** and **b** show the results of simulations for the evolution of transverse normalized emittance ε_{nx} from various initial values ε_{n0} at the initial phase $\Psi_0 = 0$ and that of the relative energy spread σ_γ/γ from the initial spread of $\sigma_\gamma/\gamma_0 = 0.1$ for various initial energies due to the effect of the radiation reaction, respectively. The effect of the multiple Coulomb scattering is shown in **Figure 6c**, indicating a significant growth of the normalized emittance in the latter half of the stage. In this simulation, the

multiple Coulomb scattering has been considered for a helium plasma with $A = 4$, $Z = 2$, and $T_e = 100$ eV. Since the normalized emittance, defined by Eq. (42), is approximately calculated as $\varepsilon_{nx} \sim |\delta x||\delta(\gamma\beta_x)|$, where δx and $\delta(\gamma\beta_x)$ are the amplitudes of the transverse displacement and dimensionless momentum, the evolution of the normalized emittance traces the envelope of the betatron oscillation of the single particle, as seen in **Figures 5** and **6**. Note that the electron motion of coupled equation in Eq. (29) includes the nonlinear damping term $-(\overline{E}_z/\gamma)(d\overline{x}/d\overline{t})$, which induces the amplitude decrease in the electron acceleration phase, while the betatron motion of the electron undergoing only a linear focusing force with a constant $\overline{K}$ is described by a simple harmonic oscillator at a constant energy $m_e c^2 \gamma$, i.e., no acceleration field $\overline{E}_z = 0$, forming the constant envelope of the betatron amplitude for the matched condition of bunch size $\sigma_x^2 = \varepsilon_{nx}/(\gamma\overline{K})^{1/2}$, for which the normalized emittance is conserved.

4. Beam dynamics in multistage two-mode mixing LPAs

4.1 Seamless stage coupling with a variable curvature plasma channel

A gas-filled capillary waveguide made of metallic or dielectric materials can make it possible to comprise a seamless staging without the coupling section, where a fresh laser pulse and accelerated particle beam from the previous stage are injected so as to minimize coupling loss in both laser and particle beams and the emittance growth of particle beams due to the mismatch between the injected beam and plasma wakefield. For dephasing limited laser wakefield accelerators, the total linac length will be minimized by choosing the coupling distance to be equal to a half of the dephasing length [9]. A side coupling of laser pulse through a curved capillary waveguide [46–48] diminishes the beam-matching section consisting of a vacuum drift space and focusing magnet beamline [9]. Furthermore, the proposed scheme comprising seamless capillary waveguides can provide us with suppression of synchrotron radiation from high-energy electron (positron) beams generated by betatron oscillation in plasma-focusing channels and delivery of remarkably small normalized emittance from the linac to the beam collision section in electron-positron linear colliders.

Since the electron beam size with a finite beam emittance causes a rapid growth in a vacuum drift space outside plasma [41], the coupling segment must be used for spatial matching of the electron beam with the transverse wakefield as well as temporal phase matching with the accelerating wakefield in a subsequent stage. A proof-of-principle experiment on two LPA stages powered by two synchronized laser pulses through the plasma lens and mirror coupling has been reported, showing that an 120 MeV electron beam from a gas jet (the first stage) driven by a 28 TW, 45 fs laser pulse was focused by a first discharge capillary as an active plasma lens to a second capillary plasma channel (the second stage), where the wakefield excited by a 12 TW, 45 fs separate laser pulse reflected by a tape-based plasma mirror with a laser-energy throughput of 80% further increased an energy gain of 100 MeV [49]. In this experiment, a trapping fraction of the electron charge coupled to the second stage was as low as 3.5% [3]. Such a poor coupling efficiency could be attributed to the plasma mirror inserted at a vacuum drift space. To avoid a rapid growth in the vacuum drift space and improve coupling efficiency, a multistage coupling using a variable curvature plasma channel [48] enables off-axial injection of a fresh laser pulse into the LPA stage without a

vacuum gap in the coupling segment; thereby an electron bunch is continuously accelerated through the plasma-focusing channel over the consecutive stages only if the temporal phase-matching between the laser and electron beams can be optimized [3].

In the propagation of a laser pulse through a curved plasma channel, the radial equilibrium position of the laser pulse is shifted away from the channel axis due to the balance between the refractive index gradient bending the light rays inward and the centrifugal force pulling them outward. As a result, the minimum of the effective plasma density, which is proportional to a guiding potential, is located outward from the channel axis [47]. Thus, a direct guiding of a laser pulse from the curved channel with a constant curvature to the straight channel causes large centroid oscillations in the straight channel even though the laser pulse is injected to the equilibrium position, leading to loss of the laser energy and electron beam transported from the previous stage as a result of off-axis interaction with plasma wakefields [48]. To diminish the mismatching at the transition from a curved channel to a straight one [3], a variable curvature plasma channel has been devised such that the equilibrium position guides the laser centroid gradually along the channel axis from the initial equilibrium position to the channel center, where the straight channel axis merges together, as shown in **Figure 7a**. A seamless acceleration in two-stage LPA coupled with a variable curvature plasma channel has been successfully demonstrated for the guided laser intensity of 8.55×10^{18} W/cm^2 (normalized vector potential a_0 = 2) by the three-dimensional particle-in-cell simulations, as shown in **Figure 7b–f**, indicating that the injection trapping efficiency increases with the initial beam energy and approaches 100% at energies higher than 2 GeV.

4.2 Betatron motion of the particle beam in the seamless multistage

For $s \gg 1$, the asymptotic form of betatron motion in Eq. (30) yields

$$\overline{x}(s) \sim \left[\overline{x}_0{}^2 + \left(\frac{2\gamma_0\beta_{x0}}{s_0\overline{E}_{z0}}\right)^2\right]^{1/2} \sqrt{\frac{s_0}{s}} \cos{(s - s_0 + \delta_0)}, \tag{43}$$

$$\beta_x(s) \sim \frac{\overline{E}_z}{2\gamma}\left[\overline{x}_0{}^2 + \left(\frac{2\gamma_0\beta_{x0}}{s_0\overline{E}_{z0}}\right)^2\right]^{1/2} \sqrt{ss_0} \sin{(s - s_0 - \delta_0)}, \tag{44}$$

where $\tan\delta_0 = 2\gamma_0\beta_{x0}/\left(s_0\overline{x}_0\overline{E}_{z0}\right)$. The variation of the betatron amplitude with respect to the initial amplitude in the k-th stage is given by

$$\left|\frac{\overline{x}(\Psi)}{\overline{x}(\Psi_{ki})}\right| \sim \sqrt{\frac{s_{ki}}{s}} = \left(\frac{\gamma_{ki}}{\gamma}\right)^{1/4}\left|\frac{\overline{E}_z(\Psi)\overline{K}(\Psi_{ki})}{\overline{E}_z(\Psi_{ki})\overline{K}(\Psi)}\right|^{1/2} \sim \left(\frac{\gamma_{ki}}{\gamma}\right)^{1/4}\left|\frac{\overline{E}_z(\Psi)}{\overline{E}_z(\Psi_{ki})}\right|^{1/2}, \tag{45}$$

where $\Psi_{ki} \leq \Psi \leq \Psi_{(k+1)i}$ ($k = 1, 2, \cdots$) is the particle phase Ψ with respect to the plasma wave, Ψ_{ki} is the initial phase, and γ_{ki} is corresponding to the initial energy of the particle in the k-th stage, respectively, assuming an approximately constant focusing strength $\overline{K}(\Psi) \sim \overline{K}(\Psi_{ki})$ over the stage. As expected, the betatron amplitude is simply proportional to $(\gamma_{ki}/\gamma)^{1/4}$ for the constant accelerating field $\overline{E}_z(\Psi)$ during the stage. In the two-mode mixing LPA system comprising the periodic accelerating structure, i.e., $\overline{E}_z(\Psi_{ki} + \Delta\Psi) = \overline{E}_z(\Psi_{li} + \Delta\Psi)$ for a phase advance $\Delta\Psi$ in the k-th and l-th stages, the ratio of the accelerating field amplitude is given by

$$\left| \frac{\overline{\overline{E}}_z(\Psi)}{\overline{E}_z(\Psi_{ki})} \right| = e^{-2\alpha_d a_0^2(\Psi - \Psi_{ki})} \left| \frac{\Omega(\Psi)}{\Omega(\Psi_{ki})} \right|, \tag{46}$$

where $\Omega(\Psi) = \cos\Psi + \sqrt{C_1 C_2}(1 + \cos 2\Psi)/(C_1 + C_2)$. In the accelerator system consisting of N_s stages, the final betatron amplitude yields

$$|\overline{x}(\Psi_f)| \sim |\overline{x}_0|\left(\gamma_0/\gamma_f\right)^{1/4} R^{N_s/2} \exp\left[-\alpha_d a_0^2(\Psi_f - \Psi_0)\right], \tag{47}$$

where Ψ_f, $m_e c^2 \gamma_f$ are the final phase and energy of the particle at the N_s-th stage, respectively, and $R = \left|\Omega(\Psi_f)/\Omega(\Psi_i)\right|$ is the ratio of the amplitude $\Omega(\Psi)$ between the final and initial phases in the single stage. If this ratio is chosen so as to be $R < \exp\left(2\alpha_d a_0^2 \Delta\Psi\right)$, the betatron amplitude will decrease as the electron propagates the accelerator stages.

Here we consider the evolution of transverse normalized emittance for the particle beam acceleration in the multistage capillary accelerator. The definition of transverse normalized emittance given by Eq. (42) is expressed as $\varepsilon_{nx}^2 = \langle \delta\overline{x}^2 \rangle \langle \delta u_x^2 \rangle - \langle \delta\overline{x}\delta u_x \rangle^2$, where $\delta\overline{x} = \overline{x} - \langle\overline{x}\rangle$ and $\delta u_x = u_x - \langle u_x \rangle$ are the deviation from the mean transverse displacement $\langle\overline{x}\rangle$ and normalized momentum $\langle u_x \rangle = \langle \gamma\beta_x \rangle$, respectively. The particle orbit undergoing betatron motion is written for $s \gg 1$ from Eqs. (43) and (44) as $\overline{x} = \overline{x}_m\sqrt{s_0/s}\cos\varphi$ and $u_x = \gamma\beta_x = \overline{x}_m\left(\overline{E}_z\sqrt{ss_0}/2\right)\sin\varphi$, where
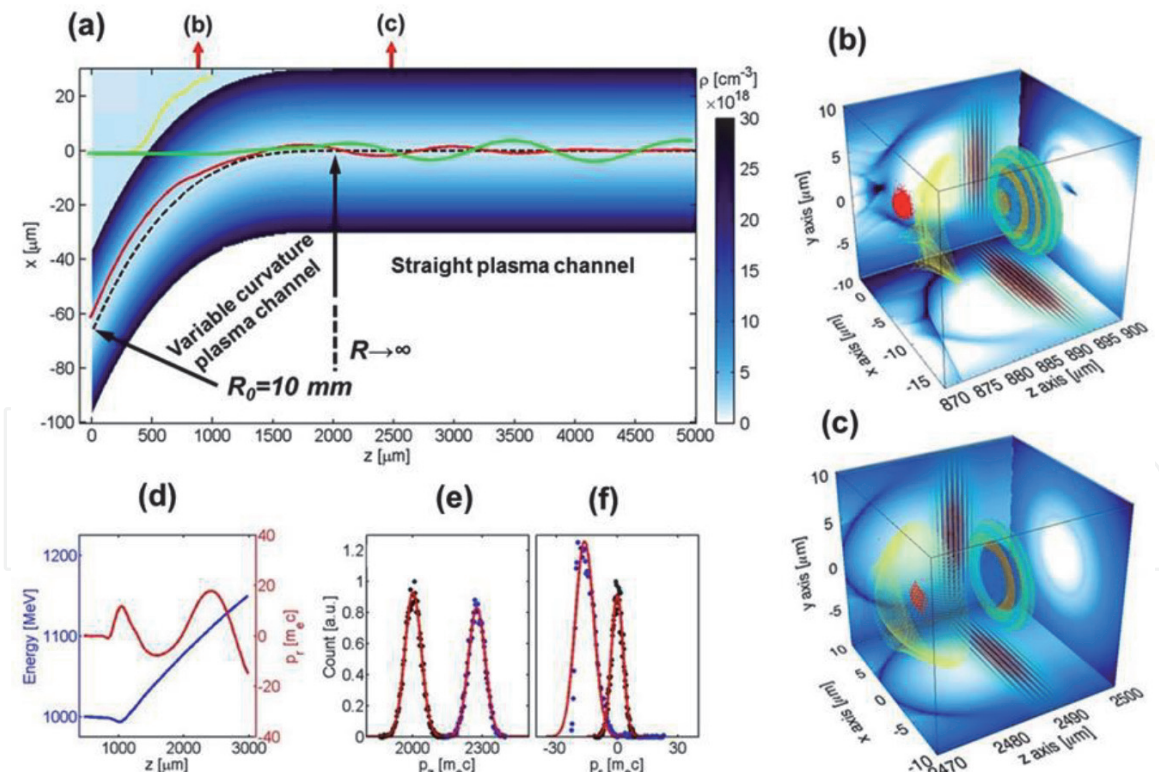

Figure 7.
(a) Geometry of the coupling segment, which is composed of a variable-curvature plasma channel with a gradually varying channel radius along the channel axis (dashed line) from the entrance radius R_o = 10 mm in the first stage to that of a straight channel $R \rightarrow \infty$ in the second stage, and the centroid trajectories for a first-stage laser (yellow), a second-stage laser (red), and an electron beam (green). When the second laser is injected at the curved channel entrance with an incidence angle of 5.7° and an off-axis deviation of 6.3 μm, its centroid trajectory and an electron bunch (red points) are seamlessly coupled to the straight plasma channel, as shown in the three-dimensional particle-in-cell (3D PIC) simulation results before (b) and after (c) the electron bunch is trapped in the second straight channel [3]. (d) Energy and transverse momentum, initial (black points) and final (blue points) (e) longitudinal and (f) transverse momentum distributions, and their Gaussian fitting curves (red) of the electron beam obtained from the simulation results.

$\varphi = \overline{\omega}_\beta \overline{t}$ is the betatron phase and $\overline{x}_m = \left[\overline{x}_0^2 + \left(2\gamma_0 \beta_{x0}/s_0 \overline{E}_{z0} \right)^2 \right]^{1/2}$. Thus, the ensemble averaged quantities $\langle \delta \overline{x}^2 \rangle$, $\langle \delta u_x^2 \rangle$, and $\langle \delta \overline{x} \delta u_x \rangle^2$ can be obtained: e.g., $\langle \delta \overline{x}^2 \rangle = \langle s_0/s \rangle \left[\langle \overline{x}_m^2 \rangle (1 + \langle \cos 2\varphi \rangle)/2 - \langle \overline{x}_m \rangle^2 \langle \cos \varphi \rangle^2 \right]$. Assuming that the energy distribution about the mean energy $\langle \gamma \rangle$, i.e., the $\delta \gamma = \gamma - \langle \gamma \rangle$ distribution, is Gaussian with a width of σ_γ, the energy is approximated about its mean value to the first order in $\delta \gamma / \langle \gamma \rangle$, i.e., $\gamma = \langle \gamma \rangle + \delta \gamma$, $\omega_\beta \simeq \omega_{\beta 0} (1 - \delta \gamma / 2 \langle \gamma \rangle)$, and $\varphi \simeq \omega_{\beta 0} \overline{t} (1 - \delta \gamma / 2 \langle \gamma \rangle)$. The ensemble averaged quantities can be calculated as averages over the distribution of energy deviations as, e.g., $\langle \cos \varphi \rangle \simeq \left(1/\sqrt{2\pi} \sigma_\gamma \right) \int_{-\infty}^{\infty} d\delta \gamma \exp \left(-\delta \gamma^2 / 2\sigma_\gamma^2 \right) \cos \left(\varphi_0 + \delta \varphi \right) = e^{-\nu_\varepsilon^2 t^2} \cos \varphi_0$, $\langle \cos 2\varphi \rangle \simeq e^{-4\nu_\varepsilon^2 t^2} \cos 2\varphi_0$, and $\langle s_0/s \rangle \simeq \left(\overline{K}_0 \overline{E}_z / \overline{K} \overline{E}_{z0} \right) (\langle \gamma_0 \rangle / \langle \gamma \rangle)^{1/2}$, where $\delta \varphi = -\varphi_0 \delta \gamma / (2\langle \gamma \rangle)$ and $\nu_\varepsilon = \omega_{\beta 0} \sigma_\gamma / \left(\sqrt{8} \langle \gamma \rangle \right)$ is the frequency corresponding to decoherence time $t_{\text{dec}} \simeq \pi \langle \gamma \rangle / \left(\omega_\beta \sigma_\gamma \right)$, defined as the time when the phase difference between the low energy part of the beam and the high-energy part is $\Delta \varphi \simeq \omega_\beta \int dt \sigma_\gamma / \langle \gamma \rangle = \pi$ [43]. Considering transverse emittance of the particle beam with initial energy spread that dominates decoherence, the normalized emittance for $t \gg t_{\text{dec}}$ is given by

$$\overline{\varepsilon}_{nx} = \frac{1}{2} \left| \frac{\overline{E}_z}{\overline{E}_{z0}} \right| \overline{K}_0 \sqrt{\langle \gamma_0 \rangle} \langle \overline{x}_{m0}^2 \rangle = \frac{1}{2} \left| \frac{\overline{E}_z}{\overline{E}_{z0}} \right| \overline{K}_0 \sqrt{\langle \gamma_0 \rangle} \left(\langle \overline{x}_0^2 \rangle + \frac{\langle u_{x0}^2 \rangle}{\overline{K}_0^2 \langle \gamma_0 \rangle} \right), \quad (48)$$

where $\overline{\varepsilon}_{nx} = k_p \varepsilon_{nx}$ is the dimensionless normalized emittance. If the beam is initially matched to the laser wakefield focusing channel, i.e., $\overline{x}_0 = 2\gamma_0 \beta_{x0} / \left(s_0 \overline{E}_{z0} \right) = u_{x0} / \left(\overline{K}_0 \sqrt{\gamma_0} \right)$, such that in the absence of radiation the beam radial envelope undergoes no betatron oscillation, the normalized emittance can be expressed as

$$\overline{\varepsilon}_{nx} = \left| \frac{\overline{E}_z}{\overline{E}_{z0}} \right| \overline{K}_0 \sqrt{\langle \gamma_0 \rangle} \langle \overline{x}_0^2 \rangle = \left| \frac{\overline{E}_z}{\overline{E}_{z0}} \right| \overline{\varepsilon}_{nx0}. \quad (49)$$

This indicates that in the absence of radiation and multiple Coulomb scattering, the transverse normalized emittance of an initially matched beam is conserved in the laser wakefield acceleration when the amplitude of accelerating field has no variation, i.e., $\left| \overline{E}_z \right| = \left| \overline{E}_{z0} \right|$. Note that the decreasing accelerating field at the final phase results in a decrease of the normalized emittance of the injected beam matched to the laser wakefield at the initial phase in the single stage. For the multistage laser wakefield acceleration without a vacuum drift space in the coupling section, properly choosing the injection and extraction phases enables continuous reduction of the normalized emittance in the absence of synchrotron radiation and multiple Coulomb scattering with plasma ions. Since the initial values of the displacement $\langle \overline{x} \rangle$ and normalized momentum $\langle u_x \rangle$ at the next stage are expressed as $\langle \overline{x}_1^2 \rangle \simeq \sqrt{\langle \gamma_0 \rangle / \langle \gamma_1 \rangle} \langle \overline{x}_m^2 \rangle_0 \overline{E}_{z1} \overline{K}_0 / (2 \overline{E}_{z0} \overline{K}_1)$ and $\langle u_{x1}^2 \rangle \simeq \overline{K}_0 \overline{K}_1 \sqrt{\langle \gamma_0 \rangle \langle \gamma_1 \rangle} \langle \overline{x}_m^2 \rangle_0 \overline{E}_{z1} / (2 \overline{E}_{z0})$ [19], the initial amplitude of betatron oscillation at the next stage is

$$\langle \overline{x}_m^2 \rangle_1 = \langle \overline{x}_1^2 \rangle + \langle u_{x1}^2 \rangle / (\overline{K}_1 \langle \gamma_1 \rangle)$$
$$= \sqrt{\langle \gamma_0 \rangle / \langle \gamma_1 \rangle} \langle \overline{x}_m^2 \rangle_0 \overline{E}_{z1} \overline{K}_0 / (\overline{E}_{z0} \overline{K}_1).$$

Accordingly, the emittance at the k-th stage is calculated as

$$\bar{\varepsilon}^k{}_{nx} = (1/2)\bar{K}(\Psi_f)\sqrt{\langle\gamma\rangle_0}\langle\bar{x}^2_m\rangle_0$$

$$\cdot\,|\bar{E}_z(\Psi_f)/\bar{E}_z(\Psi_i)|^k|\bar{K}(\Psi_i)/\bar{K}(\Psi_f)|^k.$$

Assuming $\overline{K}(\Psi_f) \approx \overline{K}(\Psi_i) = \overline{K}_0$, the dimensionless normalized emittance at the k-th stage yields

$$\bar{\varepsilon}^k{}_{nx} \simeq \frac{1}{2}\left|\frac{\overline{E}_z(\Psi_f)}{\overline{E}_z(\Psi_i)}\right|^k \overline{K}_0\sqrt{\langle\gamma\rangle_0}\langle\bar{x}^2_m\rangle_0 = \frac{1}{2}R^k e^{-2\alpha a_0^2 k\Delta\Psi}\overline{K}_0\sqrt{\langle\gamma\rangle_0}\langle\bar{x}^2_m\rangle_0 = R^k e^{-2\alpha a_0^2 k\Delta\Psi}\bar{\varepsilon}_{n0},$$

(50)

where $\left|\overline{E}_z(\Psi_f)/\overline{E}_z(\Psi_i)\right| = Re^{-2\alpha a_0^2\Delta\Psi}$ is the ratio of the accelerating field amplitude at the final phase Ψ_f to that at the initial phase Ψ_i with $R = \left|\Omega(\Psi_f)/\Omega(\Psi_i)\right|$ and $\Delta\Psi = \Psi_f - \Psi_i$. Setting $\overline{K}_0\langle\gamma_0\rangle^{1/2}\langle\bar{x}^2_m\rangle = 2\bar{\varepsilon}_{n0}$, the normalized emittance increases or decreases monotonically, depending on $R > e^{2\alpha a_0^2\Delta\Psi}$ or $R < e^{2\alpha a_0^2\Delta\Psi}$ as the particles move along the stage in the absence of radiation and multiple Coulomb scattering.

For an application of laser-plasma accelerators to electron-positron colliders, it is of most importance to achieve the smallest possible normalized emittance at the final stage of the accelerator system, overwhelming the emittance growth due to the multiple Coulomb scattering off plasma ions, being increased in proportion to the square root of the beam energy. We consider the effect of multiple Coulomb scattering on the emittance growth and evaluate an achievable normalized emittance at the end of the accelerator system comprising N_s stages. Using the growth rate of the mean square deflection angle in Eq. (36) due to the multiple Coulomb scattering, the growth rate of the transverse normalized emittance is estimated as [8, 44].

$$\frac{d\varepsilon_n^{\mathrm{SCAT}}}{dz} = \frac{1}{2}\frac{\gamma}{k_\beta}\frac{d\langle\theta^2\rangle}{dz} = \frac{k_p r_e Z}{\overline{K}\sqrt{\gamma}}\ln\left(\frac{\lambda_D}{R_N}\right),$$

(51)

where $k_\beta = K/\sqrt{\gamma}$ is the wave number of betatron oscillation. In the single stage, the transverse normalized emittance of the particles undergoing the wakefields evolves the growth in the same manner as the injected particle beam without the multiple Coulomb scattering as

$$\bar{\varepsilon}^1{}_{nx} = \left|\frac{\overline{E}_z(\Psi_1)}{\overline{E}_z(\Psi_0)}\right|\bar{\varepsilon}_{n0} + \frac{k_p r_e Z\ln(\lambda_D/R_N)}{\overline{K}_0\overline{E}_z(\Psi_0)}\left(\sqrt{\langle\gamma_{1f}\rangle} - \sqrt{\langle\gamma_{1i}\rangle}\right).$$

(52)

At the N_s-th stage, the normalized emittance can be obtained from

$$\bar{\varepsilon}^N{}_{nx} = \left|\frac{\overline{E}_z(\Psi_1)}{\overline{E}_z(\Psi_0)}\right|^N\bar{\varepsilon}_{n0} + \frac{k_p r_e Z\ln(\lambda_D/R_N)}{\overline{K}_0\overline{E}_z(\Psi_0)}\sum_{k=1}^{N}\left|\frac{\overline{E}_z(\Psi_1)}{\overline{E}_z(\Psi_0)}\right|^{N-k}\sqrt{\gamma_k}\left(1 - \sqrt{\frac{\gamma_{k-1}}{\gamma_k}}\right).$$

(53)

Assuming that the beam energy at the k-th stage is approximately given by $\langle\gamma_k\rangle \simeq (\pi C_1 C_2/2)^{1/2}a_0^2\gamma_g^2 e^{-(1+4\alpha a_0^2\Psi_0)/2}k\Delta\Psi$ for $k \gg 1$, Eq. (53) can be calculated as

$$\bar{\varepsilon}^N{}_{nx} = \bar{\varepsilon}_{n0}R^{N_s}e^{-2N_s\alpha_d a_0^2\Delta\Psi} + \left(\frac{C_1 C_2}{2\pi}\right)^{1/4}\frac{C_S Z\ln(\lambda_D/R_N)}{a_0(C_1 + C_2)}\frac{e^{(1+4\alpha a_0^2\Psi_0)/4}R^{N_s}e^{-2N_s\alpha_d a_0^2\Delta\Psi}\sqrt{\Delta\Psi}}{\overline{K}_0|\Omega(\Psi_0)|\sqrt{\ln R - 2\alpha a_0^2\Delta\Psi}}$$

$$\times\left[\mathrm{erf}\sqrt{N_s(\ln R - 2\alpha_d a_0^2\Delta\Psi)} - \mathrm{erf}\sqrt{\ln R - 2\alpha_d a_0^2\Delta\Psi}\right],$$

(54)

for $R > e^{2\alpha a_0^2 \Delta\Psi}$, where $C_S = k_p r_e \gamma_g = 17.7 \times 10^{-9} [\mu m]/\lambda_0$ and $\mathrm{erf}(x) = (2/\sqrt{\pi})\int_0^x e^{-t^2} dt$ are the error function, and for $R < e^{2\alpha a_0^2 \Delta\Psi}$,

$$\bar{\varepsilon}^N_{nx} = \bar{\varepsilon}_{n0} R^{N_s} e^{-2N_s \alpha a_0^2 \Delta\Psi} + \left(\frac{2}{\pi}\right)^{3/4} \frac{C_s (C_1 C_2)^{1/4} Z \ln(\lambda_D/R_N)}{a_0(C_1 + C_2)} \frac{e^{(1+4\alpha_d a_0^2 \Psi_0)/4}\sqrt{\Delta\Psi}}{\overline{K}_0 |\Omega(\Psi_0)|\sqrt{2\alpha_d a_0^2 \Delta\Psi - \ln R}},$$

$$\times \left\{ F\left[\sqrt{N_s (2\alpha_d a_0^2 \Delta\Psi - \ln R)}\right] - R^{N_s - 1} e^{-2(N_s - 1)\alpha_d a_0^2 \Delta\Psi} F\left[\sqrt{2\alpha_d a_0^2 \Delta\Psi - \ln R}\right] \right\}$$

(55)

where $F(x) = e^{-x^2}\int_0^x e^{t^2} dt$ is Dawson's integral. For $R = e^{2\alpha a_0^2 \Delta\Psi}$, i.e., $\left|\overline{E}_z(\Psi_f)/\overline{E}_z(\Psi_i)\right| = 1$, the normalized emittance at the N_s-th stage is simply calculated as

$$\bar{\varepsilon}^N_{nx} = \bar{\varepsilon}_n^{\,0} + \frac{k_p r_e Z \ln(\lambda_D/R_N)}{\overline{K}_0 |\overline{E}_z(\Psi_0)|}\left(\sqrt{\gamma_{N_s}} - \sqrt{\gamma_0}\right)$$

$$\sim \bar{\varepsilon}_n^{\,0} + 2\left(\frac{2C_1 C_2}{\pi}\right)^{1/4} \frac{C_S \beta_g Z \ln(\lambda_D/R_N)}{a_0(C_1 + C_2)} \frac{e^{(1+4\alpha a_0^2 \Psi_0)/4}\sqrt{N_s \Delta\Psi}}{\overline{K}_0 |\Omega(\Psi_0)|}.$$

(56)

As expected, the normalized emittance in the multistage accelerator operated with the constant accelerating field is conserved to the initial normalized emittance and then limited by an increasing growth due to multiple Coulomb scattering. For $R > e^{2\alpha a_0^2 \Delta\Psi}$, the initial emittance of the injected beam dominates an exponential growth of the normalized emittance, while for $R < e^{2\alpha a_0^2 \Delta\Psi}$, an exponential decrease of the initial emittance is followed by a slow decrease of the normalized emittance arising from the multiple Coulomb scattering [19].

4.3 Numerical studies of the single-particle dynamics in multistages

Numerical studies on transverse beam dynamics of an electron bunch accelerated in the multistage mode mixing LPA have been carried out by calculating the ensemble of trajectories of test particles throughout consecutive stages, using the single-particle dynamics code based on the analytical solutions of the equations of motion of an electron in laser wakefields with the presence of effects of the radiation reaction and multiple Coulomb scattering, as described in Section 3. **Figure 8a** shows examples of the phase space distribution of 10^4 test particles on the $k_p x - \gamma\beta_x$ plane and evolution of the transverse normalized emittance for 400 stages, in each of which the electron is accelerated between the initial wakefield phase $\Psi_i = 0$ and final phase $\Psi_f = 4.5\pi$, in the presence of the radiation reaction and multiple Coulomb scattering. **Figure 8b** is the result for 60 stages with the stage phase $0 \leq \Psi \leq 4\pi$ and **Figure 8c** for 50 stages with $-0.45\pi \leq \Psi \leq 4\pi$, taking into account only the radiation effect. The cases shown in **Figure 8a** and **b** obviously correspond to the exponential decrease of the normalized emittance with $R < \exp(2\alpha a_0^2 \Delta\Psi)$, while the case shown in **Figure 8c** corresponds to the exponential increase with $R > \exp(2\alpha a_0^2 \Delta\Psi)$. In **Figure 8a**, the exponential decrease of the normalized emittance is limited, leading to the equilibrium with the growth due to the multiple Coulomb scattering after several stages. In **Figure 8c**, the exponential increase can be limited by the radiation effects, resulting in an excess of radiation energy loss and the equilibrium with the radiation reaction after 20 stages. For the case shown in **Figure 8a**, the beam energy is accelerated up to 558.92 GeV with the relative rms
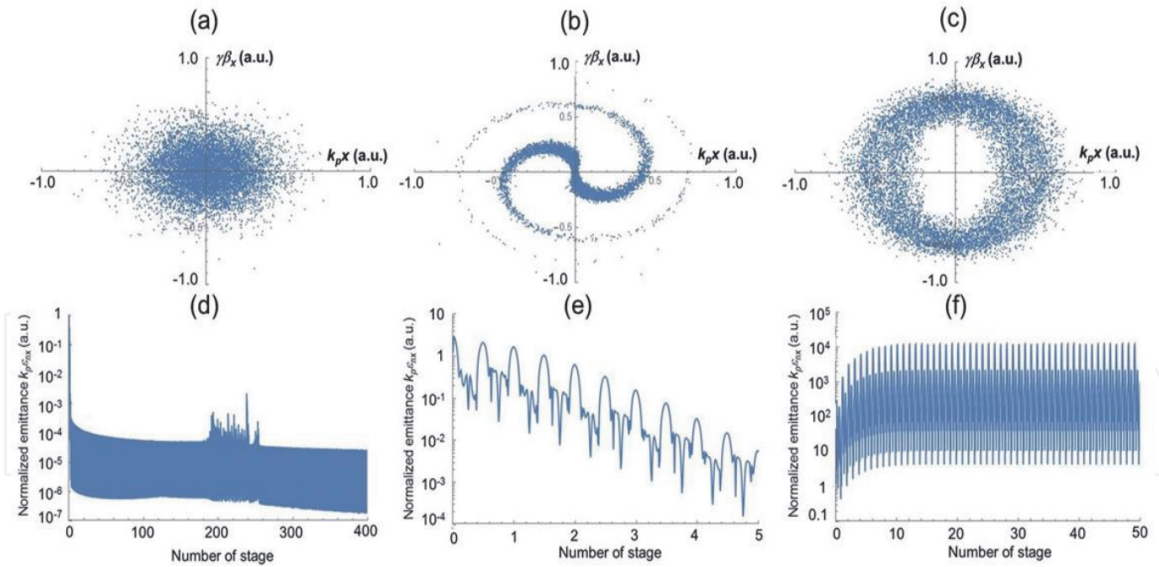
Figure 8.
*Numerical results of the beam dynamics study on the two-mode mixing multistage LPA (**Figure 1a**). (a and d) the phase space $k_p x - \gamma\beta_x$ and evolution of transverse normalized emittance $k_p\varepsilon_{nx}$ for 400 stages with each stage phase $0 \leq \Psi \leq 4.5\pi$ in the presence of radiation reaction and multiple coulomb scattering at the plasma density $n_e = 1 \times 10^{18}$ cm^{-3} and the initial normalized emittance $\varepsilon_{no} = 1$ μm. (b and e) the phase space and evolution of transverse normalized emittance (only shown for the initial 5 stages) for 60 stages with each stage phase $0 \leq \Psi \leq 4\pi$ in the presence of the radiation reaction at $n_e = 1.1 \times 10^{17}$ cm^{-3} and $\varepsilon_{no} = 100$ μm. (c and f) the phase space and evolution of transverse normalized emittance for 50 stages with each stage phase $-0.45\pi \leq \Psi \leq 4\pi$ in the presence of the radiation reaction at $n_e = 1.1 \times 10^{17}$ cm^{-3} and $\varepsilon_{no} = 100$ μm.*
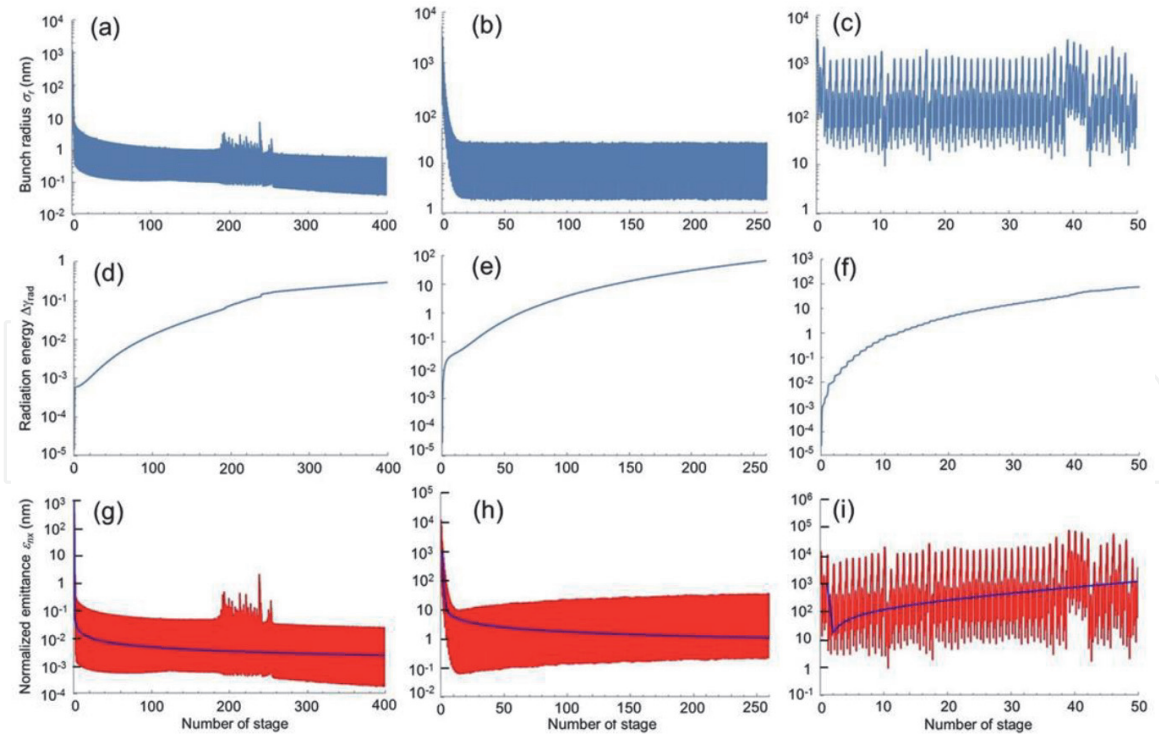
Figure 9.
Numerical results of the beam dynamics study on the two-mode mixing multistage LPA at the plasma density $n_e = 1 \times 10^{18}$ cm^{-3} and number of electrons $N_b = 1 \times 10^8$ in a bunch with a length of $k_p\sigma_z = 3$, the initial energy $m_e c^2 \gamma_0 = 1$ GeV, relative energy spread $\sigma_\gamma / \gamma_0 = 0.1$, and normalized emittance $\varepsilon_{no} = 1$ μm. (a, d, and g) evolution of rms bunch radius σ_r, radiation energy $\Delta\gamma_{rad}$, and transverse normalized emittance ε_{nx} for 400 stages with each stage phase $0 \leq \Psi \leq 4.5\pi$. (b, e, and h) evolution of the same electron beam parameters for 260 stages with each stage phase $-0.45\pi \leq \Psi \leq 4.7\pi$. (c f, and i) evolution of the same electron beam parameters for 50 stages with each stage phase $-0.45\pi \leq \Psi \leq 4.2345\pi$. In (g), (h), and (i), the blue solid curve shows a fit using the analytical emittance evolution formula in Eqs. (54) and (55).

energy spread of 0.02% over the whole 400 LPA stages with the stage phase $0 \leq \Psi \leq 4.5\pi$ at the operating plasma density of $n_e = 1 \times 10^{18}$ cm^{-3} in the accelerator length of 67 m, assuming initially a 10% relative energy spread. From this result, the beam-induced longitudinal (decelerating) wakefield becomes approximately $E_{zb}/E_0 \sim 0.01$ and focusing strength $(K_b/k_p)^2 \sim 0.12$, as calculated from an ensemble average of the radius of an electron bunch with 1×10^8 electrons and length of 16 μm, using Eqs. (20) and (26), respectively, at each step of the stage consisting of 100 segments. It is noted that both beam-induced wakefields reach the equilibrium after several stages in consistency with the evolution of the normalized emittance.

The detailed study on the evolution of the transverse normalized emittance in the multistage two-mode mixing LPA has been investigated for three cases with the different stage phases, i.e., $0 \leq \Psi \leq 4.5\pi$ (case A), $-0.45\pi \leq \Psi \leq 4.7\pi$ (case B), and $-0.45\pi \leq \Psi \leq 4.2345\pi$ (case C), the reduction coefficients $2\alpha_d a_0^2 \Delta\Psi - \ln R$ for which are 37.3, 1.37, and -0.438, respectively. **Figure 9** shows the evolution of the bunch radius σ_r (a)–(c), radiation energy $\Delta\gamma_{\text{rad}}$ (d)–(f), and transverse normalized emittance ε_{nx} (g)–(i), respectively. In **Figure 9** (g)–(i), the solid curve indicates the normalized emittance predicted from the analytical formulae of Eqs. (54) and (55), assuming that the average focusing constant is $\overline{K}_0 \sim 0.004$ for cases A–C and the growth rate is $\sim 10\%$ of the reduction coefficient for case C. It is noted that the evolution of the normalized emittance is determined by the equilibrium between the consecutive focusing and the defocusing due to the multiple Coulomb scattering at a large number of stages $N_s \gg 1$.

5. Considerations on electron-positron collider performance

Electron and positron beams being reached to the final energies in the multistage two-mode mixing LPA are extracted at a phase corresponding to the minimum transverse normalized emittance, followed by propagating a drift space in vacuum and a final focusing system to the beam-beam collisions at the interaction point. In a vacuum drift space outside plasma, the particle beam changes the spatial and temporal dimensions of the bunch proportional to the propagation distance due to the finite emittance and energy spread of the accelerated bunch. The evolution of the rms bunch envelope σ_b in vacuum without the external focusing force is given by $\sigma_b^2 = \sigma_0^2 \left[1 + (z - z_0)^2 / Z_b^2 \right]$, where σ_0 is an initial radius and $Z_b = \sigma_0^2 \gamma / \varepsilon_n$ is the characteristic distance of the bunch size growth [41]. The bunch radius after propagation of the distance L_{col} between the final LPA stage and interaction point is estimated to be $\sigma_{b^*} = \left[\sigma_{bf}^2 + \left(\varepsilon_{nf} L_{\text{col}} / \gamma \sigma_{bf} \right)^2 \right]^{1/2}$, where σ_{b^*} is the rms bunch radius at the interaction point and σ_{bf}, ε_{nf} the rms bunch radius and normalized emittance at the exit of the LPA, respectively. In collisions between high-energy electron and positron bunches from the LPAs, the beam particles emit synchrotron radiation due to the interaction, the so-called Beamstrahlung, with the electromagnetic fields generated by the counterpropagating beam. The beamstrahlung effect leads to substantial beam energy loss and degradation on energy resolution for the high-energy experiments in electron-positron linear colliders [50]. Intensive research on beamstrahlung radiation has been explored [50–52], being of relevance to the design of e$^+$e$^-$ linear colliders in the TeV center-of-mass (CM) energies, for which two major effects must be taken into account, namely, the disruption effect bending particle trajectories by the oncoming beam-generated electromagnetic fields and the

beamstrahlung effect yielding radiation loss of the particle energies induced by bending their trajectories due to the disruption [52]. The radiative energy loss due to beamstrahlung for a Gaussian beam can be estimated in terms of the beamstrahlung parameter $\Upsilon_* = 5r_e^2\gamma N_b/(12\alpha\sigma_x^*\sigma_z^*)$ for a round beam with $\sigma_{x*} = \sigma_{y*}$, where $\alpha = e^2/\hbar c$ ($\simeq 1/137.036$) is the fine-structure constant [50]. According to the beamstrahlung simulations [50], the average number of emitted photon per electron and average fractional energy loss are $n_\gamma \approx 2.54 B_\gamma\Upsilon_*/(1+\Upsilon_*^{2/3})^{1/3}$ and $\delta_b \approx 1.24 B_\gamma\Upsilon_*^2/\left[1+(3\Upsilon_*/2)^{2/3}\right]^2$, respectively, with $B_\gamma = \alpha^2\sigma_{z*}/(r_e\gamma)$. Using these parameters, the average CM energy loss can be calculated as $\Delta W/(2\gamma m_e c^2) \approx (0.44 + 0.01\log_{10}\Upsilon_*)\delta_b(1+\delta_b/n_\gamma)$. In the quantum beamstrahlung regime, the collider design must consider the CM energy loss such that their requirements can be reached as well as that of the luminosity. The geometric luminosity is given by $\mathcal{L}_0 = f_c N_b^2/(4\pi\sigma_{x*}\sigma_{y*})$, where f_c is the collision frequency. It is pointed out that an appreciable disruption effect turns out to the luminosity enhancement through the pinch effect arising from the attraction of the oppositely charged beams [51, 52]. For Gaussian beams, the disruption parameter for the round beam is $D = r_e\sigma_{z*}N_b/(\gamma\sigma_{x*}^2)$, defined as the ratio of the bunch length to the focal length of a thin lens. The luminosity enhancement factor being defined as the ratio of the effective luminosity $\mathcal{L}$ induced by the disruption to the geometric luminosity in the absence of disruption $\mathcal{L}_0$ is estimated from the empirical formula: $H_D \equiv \mathcal{L}/\mathcal{L}_0 = 1 + D^{1/4}(D^3/1+D^3)\left[\ln(\sqrt{D}+1) + 2\ln(0.8/A)\right]$, where $A = \varepsilon_n D/(r_e N)$ is the inherent divergence of the incoming beam [52]. This scenario allows us to transport both

Plasma density n_e	1×10^8 cm^{-3}
Plasma wavelength λ_p	33.4 μm
Capillary radius R_c	152.6 μm
Capillary stage length	16.75 cm
Laser wavelength λ	1 μm
Laser spot radius r_0	91 μm (51 μm)
Laser pulse duration τ	25 fs
Normalized vector potential a_0	1
Electromagnetic hybrid mode	EH$_{11}$ and EH$_{12}$
Coupling efficiency for an Airy beam (a Gaussian beam)	C$_1$ = 0.4022 (0.5980) C$_2$ = 0.4986 (0.3531)
Bunch initial and final phase	Ψ_i = 0, Ψ_f = 4.5π
Average accelerating gradient	8.3 GeV/m
Laser peak power P_L	95 TW (18 TW)
Laser pulse energy U_L	2.4 J (0.44 J)
Repetition frequency f_c	50 kHz
Laser average power per stage	120 kW (22 kW)
Laser depletion η_{pd}	77%

The parameters in () correspond to the incident laser pulse with a Gaussian beam.

Table 1.
Parameters of the two-mode mixing laser-plasma accelerator stage.

CM energy	1.12 TeV
Beam energy	559 GeV
Injection beam energy	1 GeV
Particle per bunch N_b	1×10^8
Collision frequency f_c	50 kHz
Total beam power	0.9 MW
Geometric luminosity $\mathfrak{L}_0$	3.6×10^{32} cm^{-2} s^{-1}
Effective luminosity $\mathfrak{L}$	1.76×10^{34} cm^{-2} s^{-1}
Effective CM energy	1.09 TeV
rms CM energy spread	8.4%
rms bunch length σ_z	16 μm
Beam radius at IP σ_{b*}	3.3 nm
Beam aspect ratio R	1
Normalized emittance at IP ε_{nf}	3.7 pm-rad
Distance between LPA and IP L_{col}	0.2 m
Beamstrahlung parameter Υ_*	0.94
Beamstrahlung photons n_γ	0.52
Disruption parameter D	12
Luminosity enhancement H_D	49
Number of stages per beam N_s	400
Linac length per beam	67 m
Power requirement for lasers	95 MW (18 MW)

The parameters in () correspond to the incident laser pulse with a Gaussian beam.

Table 2.
Parameters for 1 TeV laser-plasma e^+e^- linear collider.

beams into the interaction point through no extra focusing devices, which often induce the degradation of beam qualities prior to their interactions. In this scheme, the vacuum drift region from the end of the LPA to the interaction point can be used for control of the transverse beam size that strongly affect the luminosity and CM energy through the beamstrahlung radiation and disruption. A typical design example of the LPA stage using the gas-filled [19] two-mode mixing LPA operated with EH_{11} and EH_{12} is shown in **Table 1**.

An embodiment of the LPA stage may be envisioned by exploiting a tens kW-level high-average power laser such as a coherent amplification network of fiber lasers [53]. **Table 2** summarizes key parameters on the performance of 1 TeV CM energy electron-positron linear collider.

6. Conclusions

The electron acceleration and beam dynamics of the two-mode mixing LPA comprising a gas-filled metallic or dielectric capillary have been presented for the performance of the single-stage and multistage configurations. As shown in **Table 1**, when a laser pulse with an Airy beam (or a Gaussian beam) profile of the

spot radius $r_0 \simeq 0.6R_c$ ($r_0 = 0.33R_c$) is coupled to a gas-filled capillary, two electromagnetic hybrid modes EH_{11} and EH_{12} are generated with the coupling efficiency $C_1 = 0.40$ ($C_1 = 0.60$) and $C_2 = 0.50$ ($C_2 = 0.35$), respectively. Furthermore, when the capillary radius is tuned to the matching condition given by Eq. (12), the laser pulse comprising two beating hybrid modes EH_{11} and EH_{12} with a Gaussian temporal profile can efficiently excite a rectified accelerating wakefield, where relativistic electrons dominantly propagate in the accelerating phase and continuously gain the energy until depletion of the laser pulse energy, whereby a nearly 100% of the laser energy can be transferred to wakefields in the single stage.

In the two-mode mixing LPA multistage coupled with a variable curvature plasma channel, the transverse dynamics of the electron bunch is dominated by seamless recurrence of the accelerating wakefield in the stages, where the cumulative nature of the particle trajectories is determined by the amplitude ratio of the accelerating field at the final phase Ψ_f to the initial phase Ψ_i in each stage, i.e., $\left|\overline{E}_z(\Psi_f)/\overline{E}_z(\Psi_i)\right|$. With the converging condition, i.e., $\left|\overline{E}_z(\Psi_f)/\overline{E}_z(\Psi_i)\right| < 1$, the bunch radius and normalized emittance exhibit an exponential decrease initially and then turn out to be in equilibrium with the growth due to the multiple Coulomb scattering after 20 stages, leading to the rms bunch radius of the order of $\sim$1 nm and the transverse normalized emittance of the order of $\sim$0.1 nm-rad at the beam energy 559 GeV with the relative rms energy spread of 0.02% in the final 400 stage of the accelerator length of 67 m, as shown for case A in **Figure 9**. This capability of producing such high-energy and high-quality electron (or positron) beams allows us to conceive a unique electron-positron linear collider with high luminosity of the order of 10^{34} cm^{-2} s^{-1} at 1 TeV center-of-mass energy in a very compact size.

In conclusion, a novel scheme of 1 TeV electron-positron linear collider comprising properly phased multistage two-mode mixing LPAs using gas-filled capillary waveguides can provide a unique approach in collider applications. This scheme presented resorts two major mechanisms pertaining to laser wakefield acceleration, that is, dephasing and strong focusing force as well as very high-gradient accelerating field. The multistage scheme using two-mode mixing capillary waveguides filled with plasma may provide a robust approach leading to the supreme goal for LPAs. The numerical model developed for study on beam dynamics in large-scale LPAs will be useful for assessing effects of underlying physics and the optimum design for future laser-plasma-based colliders. Although the present model has been developed to study the simplest two-dimensional phase-space model of electron beam dynamics in laser wakefield acceleration, the analysis of higher multi-dimensional phase-space model as well as the quantum plasma effect will be extensively pursued in the future work.

Acknowledgements

Author details

Kazuhisa Nakajima[1*], Min Chen[1] and Zhengming Sheng[1,2]

1 Key Laboratory for Laser Plasmas (MOE), School of Physics and Astronomy, Shanghai Jiao Tong University, Shanghai, China

2 SUPA, Department of Physics, University of Strathclyde, Glasgow, UK

*Address all correspondence to: naka115@dia-net.ne.jp

IntechOpen

References

[1] Gibney E. Who will build the next LHC? Nature. 2016;**536**:383-384

[2] Schulte D. Application of advanced accelerator concepts for colliders. In: Chao AW, Chou W, editors. Review of Accelerator Science and Technology. Vol. 9. Singapore: World Scientific; 2016. pp. 209-233. DOI: 10.1142/S1793626816300103

[3] Nakajima K. Seamless multistage laser-plasma acceleration toward future high-energy colliders. Light: Science & Applications. 2018;**7**:21. DOI: 10.1038/s41377-018-0037-6

[4] Tajima T, Dawson JM. Laser electron accelerator. Physical Review Letters. 1979;**43**:267-270. DOI: 10.1103/PhysRevLett.43.267

[5] Nakajima K. In: Chao AW, Chou W, editors. Review of Accelerator Science and Technology. Vol. 9. Singapore: World Scientific; 2016. pp. 19-61. DOI: 10.11412/S1793626816300024

[6] Grüner F, Becker S, Schramm U, Eichner T, Fuchs M, Weingartner R, et al. Design considerations for table-top, laser-based VUV and X-ray free electron lasers. Applied Physics B: Lasers and Optics. 2007;**86**:431-435. DOI: 10.1007/s00340-006-2565-7

[7] Nakajima K. Compact X-ray sources-towards a table-top free-electron laser. Nature Physics. 2008;**4**:92-93

[8] Schroeder CB, Esarey E, Geddes CGR, Benedetti C, Leemans WP. Physics considerations for laser-plasma linear colliders. Physical Review Accelerators and Beams. 2010; **13**:101301. DOI: 10.1103/PhysRevSTAB.13.101301

[9] Nakajima K, Deng A, Zhang X, Shen B, Liu J, Li R, et al. Operating plasma density issues on large-scale laser-plasma accelerators toward high-energy frontier. Physical Review Accelerators and Beams. 2011;**14**:091301. DOI: 10.1103/PhysRevSTAB.14.091301

[10] Nakajima K, Lu HY, Zhao XY, Shen BF, Li RX, Xu ZZ. 100-GeV large scale laser plasma electron acceleration by a multi-PW laser. Chinese Optics Letters. 2013;**11**:013501. DOI: 10.3788/COL201311.013501

[11] Liu JS, Xia CQ, Wang WT, Lu HY, Wang C, Deng AH, et al. All-optical cascaded laser wakefield accelerator using ionization-induced injection. Physical Review Letters. 2011;**107**:035001. DOI: 10.1103/PhysRevLett.107.035001

[12] Wang X, Zgadzaj R, Fazel N, Li Z, Yi SA, Zhang X, et al. Quasi-monoenergetic laser-plasma acceleration of electrons to 2 GeV. Nature Communications. 2013;**4**:1988-1-1988-9. DOI: 10.1038/ncomms2988

[13] Kim HT, Pae KH, Cha HJ, Kim IJ, Yu TJ, Sung JH, et al. Enhancement of electron energy to the multi-GeV regime by a dual-stage laser-wakefield accelerator pumped by petawatt laser pulses. Physical Review Letters. 2013; **111**:165002. DOI: 10.1103/PhysRevLett.111.165002

[14] Kim HT, Pathak VB, Pae KH, Lifschitz A, Sylla F, Shin JH, et al. Stable multi-GeV electron accelerator driven by waveform-controlled PW laser pulses. Scientific Reports. 2017;**7**:1020. DOI: 10.1038/s41598-017-09267-1

[15] Leemans WP, Gonsalves AJ, Mao HS, Nakamura K, Benedetti C, Schroeder CB, et al. Multi-GeV electron beams from capillary-discharge-guided subpetawatt laser pulses in the self-trapping regime. Physical Review Letters. 2014;**113**:245002. DOI: 10.1103/PhysRevLett.113.245002

[16] Lu H, Liu M, Wang W, Wang C, Liu J, Deng A, et al. Laser wakefield acceleration of electron beams beyond 1 GeV from an ablative capillary discharge waveguide. Applied Physics Letters. 2011;**99**:091502. DOI: 10.1063/1.3626042

[17] Gonsalves AJ, Nakamura K, Daniels J, Benedetti C, Pieronek C, de Raadt TCH, et al. Petawatt laser guiding and electron beam acceleration to 8 GeV in a laser-heated capillary discharge waveguide. Physical Review Letters. 2019;**122**:084801. DOI: 10.1103/PhysRevLett.122.084801

[18] Osterhoff J, Popp A, Major Z, Marx B, Rowlands-Rees TP, Fuchs M, et al. Generation of stable low-divergence electron beams by laser-wakefield acceleration in a steady-state-flow gas cell. Physical Review Letters. 2008;**101**:085002. DOI: 10.1103/PhysRevLett.101.085002

[19] Nakajima K, Wheeler J, Mourou G, Tajima T. Novel laser-plasma TeV electron-positron linear colliders. International Journal of Modern Physics A. 2019;**34**:1943003. DOI: 10.1142/S0217751X19430036

[20] Cros B, Courtois C, Matthieussent G, Bernardo AD, Batani D, Andreev N, et al. Eigenmodes for capillary tubes with dielectric walls and ultraintense laser pulse guiding. Physical Review E. 2002;**65**:026405. DOI: 10.1103/PhysRevE.65.026405

[21] Nakajima K. Laser electron acceleration beyond 100 GeV. The European Physical Journal Special Topics. 2014;**223**:999-1016. DOI: 10.1140/epjst/e2014-02151-9

[22] Behnke T, Brau TJE, Foster B, Fuster J, Harrison M, Paterson JM, et al., editors. The international linear collider accelerator. In: The International Linear Collider Technical Design Report. Vol. 1. 2013. pp. 9-26

[23] Durfee CG III, Milchberg HM. Light pipe for high intensity laser pulses. Physical Review Letters. 1993;**71**:2409. DOI: 10.1103/PhysRevLett.71.2409

[24] Xiao YF, Chu HH, Tsai HE, Lee CH, Lin JY, Wang J, et al. Efficient generation of extended plasma waveguides with the axicon ignitor-heater scheme. Physics of Plasmas. 2004;**11**:L21-L24. DOI: 10.1063/1.1695354

[25] Levin M, Pukhov A, Zigler A, Sugiyama K, Nakajima K, Hubbard RF, et al. Long plasma channels in segmented capillary discharges. Physics of Plasmas. 2006;**13**:083108. DOI: 10.1063/1.2261853

[26] Liu MW, Deng AH, Liu JS, Li RX, Xu JC, Xia CQ, et al. Note: Low density and long plasma channels generated by laser transversely ignited ablative capillary discharges. The Review of Scientific Instruments. 2009;**81**:036107. DOI: 10.1063/1.3360925

[27] Hosokai T, Kando M, Dewa H, Kotaki H, Kondo S, Hasegawa N, et al. Optical guidance of terawatt laser pulses by the implosion phase of a fast Z-pinch discharge in a gas-filled capillary. Optics Letters. 2000;**25**:10-12

[28] Gonsalves AJ, Rowlands-Rees TP, Broks BHP, van der Mullen JJAM, Hooker SM. Transverse interferometry of a hydrogen-filled capillary discharge waveguide. Physical Review Letters. 2007;**98**:025002. DOI: 10.1103/PhysRevLett.98.025002

[29] Gonsalves AJ, Liu F, Bobrova NA, Sasorov PV, Pieronek C, Daniels J, et al. Demonstration of a high repetition rate capillary discharge waveguide. Journal of Applied Physics. 2016;**119**:033302. DOI: 10.1063/1.4940121

[30] Ju J, Svensson K, Döpp A, Ferrari HE, Cassou K, Neveu O, et al. Enhancement of x-rays generated by a

guided laser wakefield accelerator inside capillary tubes. Applied Physics Letters. 2012;**100**:191106. DOI: 10.1063/1.4712594

[31] Curcio A, Petrarca M, Giulietti D, Ferrario M. Numerical and analytical models to study the laser-driven plasma perturbation in a dielectric gas-filled capillary waveguide. Optics Letters. 2016;**41**:4233-4236. DOI: 10.1364/OL.41.004233

[32] Du D, Liu X, Korn G, Squier J, Mourou G. Laserinduced breakdown by impact ionization in SiO2 with pulse widths from 7 ns to 150 fs. Applied Physics Letters. 1994;**64**:3071-3073. DOI: 10.1063/1.111350

[33] Veysman M, Andreev NE, Cassou K, Ayoul Y, Maynard G, Cros B. Theoretical and experimental study of laser beam propagation in capillary tubes for non-symmetrical coupling conditions. Journal of the Optical Society of America B: Optical Physics. 2010;**27**:1400-1408

[34] Andreev NE, Cros B, Maynard G, Mora P, Wojda F. Coupling efficiency of intense laser pulses to capillary tubes for laser wakefield acceleration. IEEE Transactions on Plasma Science. 2008;**36**:1746-1750. DOI: 10.1109/TPS.2008.927144

[35] Esarey E, Schroeder CB, Leemans WP. Physics of laser-driven plasma-based electron accelerators. Reviews of Modern Physics. 2009;**81**:1229-1284. DOI: 10.1103/RevModPhys.81.1229

[36] Sprangle P, Esarey E, Ting A. Nonlinear theory of intense laser-plasma interactions. Physical Review Letters. 1990;**64**:2011-2014

[37] Shadwick BA, Schroeder CB, Esarey E. Nonlinear laser energy depletion in laser-plasma accelerators. Physics of Plasmas. 2009;**16**:056704. DOI: 10.1063/1.3124185

[38] Lu W, Huang C, Zhou MM, Mori WB, Katsouleas T. Limits of linear plasma wakefield theory for electron or positron beams. Physics of Plasmas. 2005;**12**:063101. DOI: 10.1063/1.1905587

[39] Panofsky WKH, Wenzel WA. Some considerations concerning the transverse deflection of charged particles in radio-frequency fields. The Review of Scientific Instruments. 1956;**27**:967. DOI: 10.1063/1.1715427

[40] Chen P, Su JJ, Katsouleas T, Wilks S, Dawson JM. Plasma focusing for high-energy beams. IEEE Transactions on Plasma Science. 1987;**PS-15**:218-225

[41] Khachatryan AG, Irman A, van Goor FA, Boller KJ. Femtosecond electron-bunch dynamics in laser wakefields and vacuum. Physical Review Accelerators and Beams. 2007;**10**:121301. DOI: 10.1103/PhysRevSTAB.10.121301

[42] Jackson JD. Classical Electrodynamics. 3rd ed. New York: John Wiley & Sons; 1999

[43] Michel P, Schroeder CB, Shadwick BA, Esarey E, Leemans WP. Radiative damping and electron beam dynamics in plasma-based accelerators. Physical Review E. 2006;**74**:026501. DOI: 10.1103/PhysRevE.74.026501

[44] Kirby N, Berry M, Blumenfeld I, Hogan MJ, Ischebeck R, Siemann R. Emittance growth from multiple coulomb scattering in a plasma wakefield accelerator. In: Proceedings of Particle Accelerator Conference 2007 (PAC2007); Albuquerque. New Mexico, USA: IEEE; 2007. pp. 3097-3099

[45] Deng A, Nakajima K, Liu J, Shen B, Zhang X, Yu Y, et al. Electron beam

dynamics and self-cooling up to PeV level due to betatron radiation in plasma-based accelerators. Physical Review Accelerators and Beams. 2012; **15**:081303. DOI: 10.1103/PhysRevSTAB. 15.081303

[46] Ehrlich Y, Cohen C, Zigler A, Krall J, Sprangle P, Esarey E. Guiding of high intensity laser pulses in straight and curved plasma channel experiments. Physical Review Letters. 1996;**77**:4186-4189

[47] Reitsma AJW, Jaroszynski DA. Propagation of a weakly nonlinear laser pulse in a curved plasma channel. Physics of Plasmas. 2007;**14**:053104. DOI: 10.1063/1.2731816

[48] Luo J, Chen M, Wu WY, Weng SM, Sheng ZM, Schroeder CB, et al. Multistage coupling of laser-wakefield accelerators with curved plasma channels. Physical Review Letters. 2018; **120**:154801. DOI: 10.1103/ PhysRevLett.120.154801

[49] Steinke S, Tilborg J, Benedetti C, Geddes CGR, Schroeder CB, Daniels J, et al. Multistage coupling of independent laser-plasma accelerators. Nature. 2016;**530**:190-193. DOI: 10.1038/nature16525

[50] Noble RJ. Beamstrahlung from colliding electron-positron beams with negligible disruption. Nuclear Instrumentation and Methods. 1987;**256**: 427-433

[51] Hollebeek R. Disruption limits for linear colliders. Nuclear Instruments & Methods. 1981;**184**:333-347

[52] Chen P, Yokoya K. Disruption effects from the interaction of round e^+e^- beams. Physical Review D. 1988;**38**: 987-1000

[53] Wheeler J, Mourou G. Tajima T. In: Chao AW, Chou W, editors. Review of Accelerator Science and Technology.

Vol. 9. Singapore: World Scientific; 2016. pp. 151-163. DOI: 10.1142/ S1793626816300073